THE UNIVERSITY OF MICHIGAN
COLLEGE OF ENGINEERING
Department of Mechanical Engineering

Semiannual Report

USE OF ACOUSTIC EMISSION IN NONDESTRUCTIVE TESTING

March 1, 1970 - August 31, 1970

C. Bill
Frederick

01971

under contract with:

UNITED STATES AIR FORCE
AIR FORCE SYSTEMS COMMAND
AERONAUTICAL SYSTEMS DIVISION
CONTRACT NO. F33615-68-C-1703
WRIGHT-PATTERSON AIR FORCE BASE, OHIO

ARPA Order No. 1244
Program Code No. 8D10

administered through:

OFFICE OF RESEARCH ADMINISTRATION ANN ARBOR

December 1971

en gn

UMR6483

FOREWORD

This is the fourth semiannual report on a study of the use of acoustic emission in nondestructive testing. This research is supported by the Advanced Research Project Agency of the Department of Defense and is monitored by the Air Force Materials Laboratory, MANN, under Contract No. F33615-68-C-1703, initiated under ARPA Order 1244, Program Code 8D10. Mr. R. R. Rowand (MANN) is project engineer. This report covers the period from March 1, 1970 to August 31, 1970.

The program is being carried out in the Rheology and Fracture Laboratories of the Mechanical Engineering Department of The University of Michigan. The work is under the direction of Associate Professor J. R. Frederick, Professor David K. Felbeck, Mr. Robert Bill, Mr. Charles Thomas, and Mr. William Bracht have participated in the program.

ABSTRACT

Acoustic emission may be defined as the noise given off spontaneously by solid materials as a result of a sudden relaxation of stresses within the material. Stress relaxation can occur as a result of the nucleation or propagation of cracks, or as a consequence of various elastic or plastic deformation processes. The principal elastic or plastic deformation mechanisms that are sources of acoustic emission in solids are (1) the slip of existing dislocations in a metal, (2) the activation of dislocation sources, (3) twinning, and (4) grain boundary slip. This report describes the results of an investigation into the effects of one microstructure parameter, namely grain size, on acoustic emission.

TABLE OF CONTENTS

LIST OF TABLES

LIST OF FIGURES

LIST OF FIGURES (Concluded)

1.0 INTRODUCTION

Acoustic emission that results from the application of a stress to material is the result of deformation mechanisms operating in the material. Some of these mechanisms involve dislocation motion. Others result from the nucleation and growth of cracks under the applied stress. The development of fatigue and creep damage results in acoustic emission. In general, any mode of deformation which results in a sudden relaxation of stress is a potential source of acoustic emission.

The amount of acoustic emission that is observed will depend on the microstructure of the material. Therefore it is of importance to acquire some knowledge of the effect of microstructure on acoustic emission. This report describes some effects of one microstructure variable, namely grain size, on acoustic emission.

The plastic strain that metals undergo can be described as either microstrain or macrostrain.

The upper and lower limits of the plastic microstrain regime are rather arbitrarily defined as being 5×10^{-4} and 5×10^{-7} respectively. Cumulative strains smaller than 5×10^{-7} are difficult to measure with devices currently in use, and strains greater than 5×10^{-4} are easily measured with conventional dial gauges. The plastic microstrain behavior of most metals is described by models which do not apply in the regime of macrostrain. Strains of about 5×10^{-4} mark the general point at which the transition from microplastic to macrostrain behavior occurs.

There is considerable uncertainty as to what mechanisms operate during the microstrain regime, and how important grain boundaries are as dislocation obstacles during microstrain. It is not known whether microstrain proceeds

as the result of general movement of mobile or loosely pinned dislocation segments, or by the activation of dislocation sources, or possibly both. The acoustic emission technique may provide some interesting information concerning the processes involved during microstrain and the transition from microstrain to macrostrain.

A model for microstrain has been suggested by Bilello and Metzger[1]. They envision that microstraining proceeds in the following manner. Potentially mobile dislocation segments have a uniformly distributed activation stress σ_A, ranging from σ_o at the onset of microstrain, to σ_I at the end of the microstrain range. The glide distance ℓ_m of an activated segment is proportional to $(\sigma-\sigma_A)$. It is assumed that there are N_I potentially mobile dislocation segments per unit volume. Each stress increment $d\sigma_A$ activates a fraction $\frac{1}{(\sigma_I-\sigma_o)}$ of the N_I sources, and the glide distance is given by

$$\ell_m = \frac{\ell_I(\sigma-\sigma_A)}{(\sigma_I-\sigma_A)}, \tag{1.1}$$

where ℓ_I is the maximum glide distance at the end of the microstrain range. These assumptions lead to the following relationship for stress vs. microstrain:

$$\varepsilon = mN_I bC\ell_o\ell_I(\sigma-\sigma_o)^2 \,/\, 2(\sigma_I-\sigma_o)^2. \tag{1.2}$$

where m is the Schmid factor, b is the burgers vector, and C is a constant $\simeq 10$.

Experimental data obtained by Bilello and Metzger[1] on 99.999% Cu show that ε is proportional to $(\text{stress})^2$ in the microstrain range and is

independent of grain size.

Microstrain therefore ends when a substantial fraction of the primary segments undergo forward motion, and an overlapping of clear zones of adjacent segments occurs. Thus, the end of the microstrain range occurs at a strain that is dependent on initial dislocation density.

1.1 MACROSTRAIN MECHANISMS. DISLOCATION GRAIN BOUNDARY INTERACTIONS.

The theoretical strength of a grain boundary depends on the mechanism by which dislocations are envisioned to cross the boundary. These mechanisms are discussed by Li[2] who shows how they explain the rather universally valid Petch Equation,

$$\sigma = \sigma_o + K\ell^{-1/2} \tag{1.3}$$

where K is the "Petch slope", ℓ is the grain size, and σ is the yield stress. The value of K is given by Hall and Petch as

$$K = \left[\frac{\sigma_i \mu b \ell}{\pi(1-\nu)\ell_p}\right]^{1/2} \tag{1.4}$$

where σ_i is the strength of a grain boundary, ℓ_p is the pile-up length, b is Burgers Vector, μ is the shear modulus, and ν is Poisson's Ratio. If the assumption is made that $\ell_p = 1/2\ \ell$, then K is not a function of grain size.

Li[2] describes a mechanism first proposed by Cottrell by which slip in one grain initiates slip in a neighboring grain. Suppose that a dislocation pile-up is held up by a grain boundary. One can then envision a Frank-Read source located a distance ℓ_s from the boundary in the neighboring

grain. The following relation for K is obtained:

$$K = \sigma_p(\ell_s)^{1/2}, \tag{1.5}$$

where σ_p is the stress required to activate the Frank-Read source. Thus, Cottrell's interpretation of the Petch equation states that yielding occurs in a polycrystal when the stress at the head of a pile-up becomes large enough to activate a hypothetical Frank-Read source in the neighboring grain, a distance ℓ_s from the grain boundary.

Sub-grain boundaries may be able to act as sources of mobile dislocations, even in the absence of dislocation pile-ups forming against them. Dislocations may be generated by one of the three following mechanisms.

1. For small angles of mis-orientation, unpinned dislocations may be separated from those that are pinned. The strength of such a boundary is

$$\sigma_i = \frac{2\mu\theta}{n(1-\nu)} \tag{1.6}$$

where n is the ratio of free dislocations to pinned dislocations in the boundary, and θ is the misorientation angle across the sub-grain boundary.

2. When σ_i exceeds a critical value, pinned dislocations can break free instead of being left behind. If the break-away stress for pinned dislocations is σ_p, the required applied stress is σ_p/n.

3. If all dislocations are free, the stress required to move them from junctions with other sub-boundaries is

$$\sigma_i \approx \frac{2\mu b}{\pi\ell'(1-\nu)} \tag{1.7}$$

where ℓ' is the average diameter of a sub-grain.

When the dislocations break away from a sub-grain boundary, they form a forest which approximately forms a hemisphere around the sub-grain boundary. The applied shear stress required to move dislocations through this forest is

$$\sigma = \sigma_o + \frac{\mu b}{2\pi(1-\nu)} \left[\frac{8\theta}{\pi b}\right]^{1/2} \ell'^{-1/2}. \qquad (1.8)$$

Now, if $\ell_s \simeq {}^{b}/_{\theta}$, a comparison between Cottrell's mechanism, Eq. (1.5) and the value of K in Eq. (1.8) gives $\sigma_p \simeq \frac{.51\mu\theta}{\pi(1-\nu)}$ for the strength of a sub-boundary. Hence, for sub-boundaries in general, the following three stresses are nearly equivalent:

1. the stress required to drive a pile-up through a simple tilt boundary;
2. the stress required to activate a Frank-Read source in the neighboring sub-grain;
3. the stress required to move unpinned dislocations through the generated, hemispherical forest.

A grain boundary ledge mechanism has been proposed as a possible dislocation source. Presumably, a pile-up forces the formation of a ledge, or step, in a grain boundary, thus providing dislocations for intergranular slip. If the ledge density is m (number of ledges per unit length of boundary), a dislocation forest extends to form a hemisphere around the grain boundary. The density of this forest is $8m/\pi\ell$. The flow stress is given by

$$\sigma = \sigma_o + \alpha\mu b\left[\frac{8m}{\pi}\right]^{1/2} \ell^{-1/2}. \qquad \alpha \simeq 0.4. \qquad (1.9)$$

Equation (1.9) is equivalent to Eq. (1.4) if $\sigma_i = 8\alpha^2\mu b(1-\nu)m\ell_p/\ell$. The Cottrell model, Eq. (1.5), is equivalent to the ledge model if $\ell_s \approx 1/m$.

From the consideration given to many models describing the propagation of slip across a grain boundary, it is seen that they are all consistent with the Petch equation. Little difference exists among the grain boundary strengths predicted by the various models.

2.0 EXPERIMENTAL PROCEDURES

2.1 Description of the Electronic Equipment

A detailed description of the electronic equipment is given in Ref. (3). All testing was done in the 120 to 180 kHz bandwidth with the use of a Dunegan DRC 02 transducer to detect the acoustic emission.

The signal from the transducer was fed into the PAR CR-4A preamplifier where it underwent a gain of 40 dB. The bandpass setting of the CR-4 was 100 to 300 kHz. Next, the signal went through a second stage of filtering where the bandwidth was narrowed to the range 120 to 180 kHz. It then underwent a further gain of 40 dB on a Millivac VS-68B amplifier, for a total gain of 10^4. The signal was then displayed on an oscilloscope, and sent to an electronic counter. The reading on the counter was converted to a voltage by the digital-analog converter, and displayed on the y-axis of the chart recorder. The x-axis displayed the load on the specimen.

The overall background noise had an RMS value of about 6 microvolts at the preamplifier input. The amplitude of the smallest pulse to be registered on the counter was controlled by setting the trigger level of the counter. Normally, a trigger level setting of 0.1 volt was used for testing purposes, which meant that a signal had to have an amplitude of 0.1v or greater at the counter, or ten microvolts at the preamplifier input to be registered.

2.2 METHOD OF APPLYING A LOAD TO THE SPECIMEN

Fig. (2.1) is a schematic diagram of the specimen loading system. This system was used in order to obtain as low a background noise-level as possible. The load is applied to the specimen by lowering tank "a". This causes the water level in the outer tank "b" to go down, which in turn results in the lowering of the inner tank "c". Through the lever action of the beam "d", a tensile load is applied to the specimen. This equipment is located in an acoustically isolated and electrically shield "audiometrie room, except for tank "a".

The load on the specimen was measured by a set of strain gauges bonded to a simple beam, "e", which is subjected to bending when tension is applied to the specimen.

2.3 PREPARATION OF THE SPECIMENS

Most of the work being reported here was done on 99.99% Al and 99.9% Cu specimens. The test specimens were 0.12-inch thick and 4 1/2-inch long, and had a gauge section 1/4 inch wide and about 2 inches long.

Various grain size were produced in the 99.99% Al and 99.9 Cu by straining the original material from which the test specimens were made and then subsequently annealing it. Tables 2.1 and 2.2 show the amounts of strain and the heat treatments that were given to the materials.

A guide to the general procedures that were followed can be found in Ref. (4). However, the actual treatments used to achieve a given grain size were determined by experiment.

In addition to conventional grain size and sub-grain size measurements, surface examinations were performed to observe slip lines, and dislocation etch pit studies were done. Specimens in which slip were to be observed were electro-polished prior to testing. The investigation of

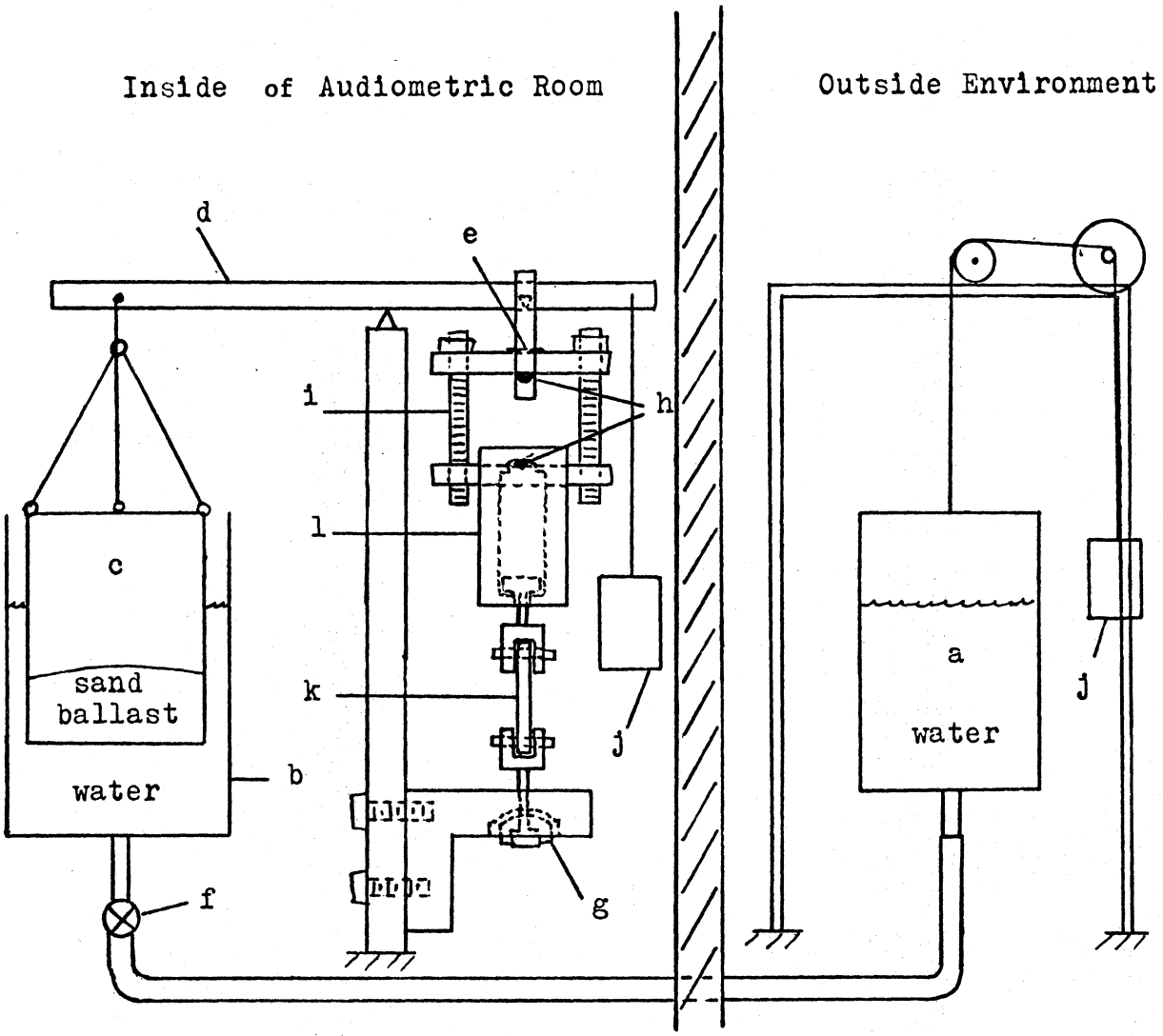

a. loading tank
b. outer tank
c. inner floating tank
d. lever action beam
e. strain gage load cell
f. flow rate control valve
g. nylon ball joint
h. teflon seated ball joints
i. adjusting turnscrews
j. counterweights
k. specimen

Figure 2.1 Diagram of the loading system.

TABLE 2.1

RESULTS OF GRAIN GROWTH PROCESSES FOR 99.99% ALUMINUM

Original Treatment	Further Treatment	Average Grain Size
20% cold rolled 3 hours at 350° C		350 μ
20% cold rolled 3 hours at 350° C	1 to 2% elongation 1½ hours at 400° C	100 to 200 μ
20% cold rolled 2 hours at 250° C		20 μ sub-grains
20% cold rolled 2 hours at 250° C	0.3% elongation 3 hours at 400° C	200 to 300 μ
20% cold rolled 2 hours at 250° C	0.3% elongation 24 hours at 620° C	700 to 800 μ
80% cold rolled 3 hours at 350° C		650 μ
80% cold rolled 3 hours at 350° C	1 to 2% elongation 24 hours at 620° C	500 to 1000 μ
80% cold rolled 2 hours at 250° C		5 μ to 10 μ sub-grains
80% cold rolled 2 hours at 250° C	0.3% elongation 10 hours at 400° C	300 to 400 μ
80% cold rolled 2 hours at 250° C	0.3% elongation 16 hours at 400° C	400 to 500 μ
80% cold rolled 2 hours at 250° C	0.3% elongation 1½ hours at 400° C	100 to 200 μ

TABLE 2.2

RESULTS OF GRAIN GROWTH PROCESSES FOR 99.9% COPPER

Reduction in Area	Heat Treatment	Average Grain Size
75%	2 hours at 350°C	10 to 15 μ
75%	3 hours at 500°C	50 μ
75%	3 hours at 900°C under vacuum	100 μ
20%	2 hours at 350°C	30 to 40 μ

the development of slip lines with increasing stress was conducted by interrupting a standard tensile test at pre-selected stress levels, and photographing the surface of the specimen.

Dislocation etch pit studies were done on 99.99% Al specimens for two purposes. One was to observe any variation in dislocation density and distribution owing to the different heat treatments that were given to the specimens. The other purpose was to gather data on the formation of dislocation pile-ups and multiplication of dislocations with plastic strain. To achieve the latter purpose, etching was done while the specimen was actually under stress. The etchant used to observe the dislocation etch pits was composed of 50% HCl, 47% HNO_3 and 3% HF.

Three 2024-T4 aluminum alloy specimens were also prepared. They were machined directly from 0.125-inch flat stock. The effects of solution treatment and aging operations on the 120 to 180 kHz acoustic emission behavior were then observed.

The orientation of the tensile axes of the single crystals that were grown were determined by the Laue back reflection x-ray technique. Some single crystals were found to be oriented for single slip and others for multiple slip. It was observed that a specimen oriented for multiple slip showed an acoustic emission behavior distinctly different from that of a specimen oriented for single slip. This behavior is described in Section (3.2.3).

3.0 RESULTS

3.1 THE EFFECT OF QUENCHED-IN VACANCIES ON THE ACOUSTIC EMISSION BEHAVIOR OF 99.99% AL

Two similar specimens of 99.99% Al were heated to 630°C for 2 hours. One specimen was then quenched to -10°C in ice brine, and immediately

tested for acoustic emission activity, while the other specimen was allowed to air cool before being tested. The experiment was then repeated with the same two specimens, except that the roles of the two specimens were switched, and the quenched specimen was allowed to age for 3 hours at room temperature. The 3-hour aging treatment enabled the quenched-in vacancies to diffuse through the lattice and form vacancy clusters, or discs. These disc were probably on the order of 200 $\mathring{A}$ in diameter, and spaced about 0.1μ to 0.5μ apart[5].

The results of the experiment show that the acoustic emission activity is grossly reduced by the presence of quenched-in vacancies. The presence of discs causes a further reduction in acoustic emission activity. These effects are clearly observable in Fig. (3.1).

3.2 DESCRIPTION OF THE ACOUSTIC EMISSION OBSERVED IN 99.99% AL

The characteristics of the emissions observed varies according to whether sub-grains are present in the material or not. In the specimens with 10μ or 20μ sub-grains (Table 2.1), most of the emissions observed are of the isolated "burst" type. The time interval between such bursts is on the order of milliseconds, Long intervals of inactivity, on the order of seconds, are observed in which no bursts at all occur.

In specimens lacking a sub-grain structure, the characteristics of the emissions are not observed to depend on grain size. The emission seems to be made up of groups of bursts in which the individual bursts are separated by 10 to 100 microseconds. The groups contain 10 to 100 bursts and usually re-occur at a fairly uniform rate. They result in the "steps" in the high-rate-of-emission" part of the Σ LE versus applied stress plots, as may be seen in Fig. (3.2). In the intervals between the groups of bursts, a segment of low-rate-or-emission is often observed.

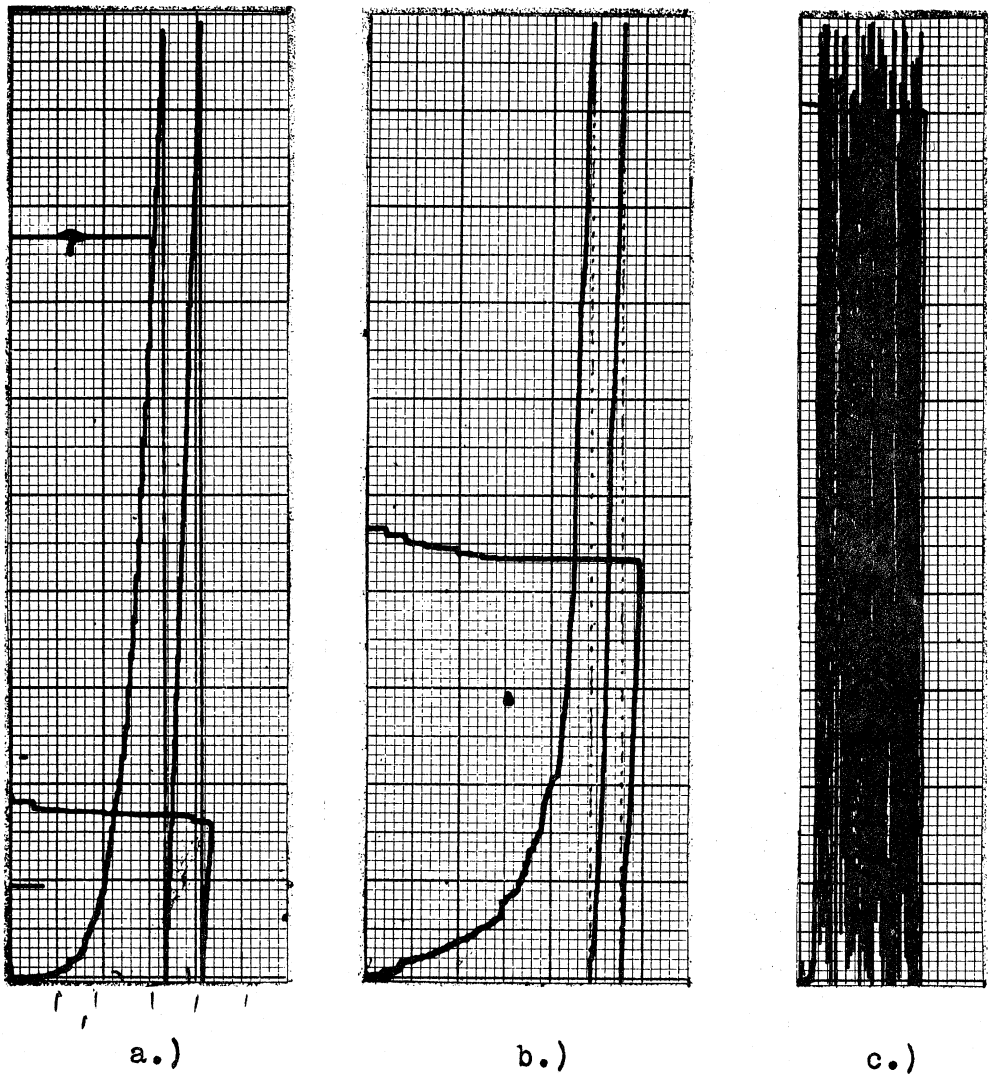

Figure 3.1. ΣLE versus applied stress for a.) a specimen which was quenched from 630°C to -10°C, then tested within 2 minutes; b.) a specimen which was quenched as in a.), then allowed to age at room temperature for 3 hours before being tested; c.) a specimen which was air cooled from 630°C. Each ½ inch square on the horizontal scale represents a 750psi applied stress increment above a 750psi preload. The vertical (ΣLE) scale is 10,000 counts per full scale deflection of the pen, or 1000 counts per ½ inch division. (The frequency range used in these tests was 8 to 15 kHz.)

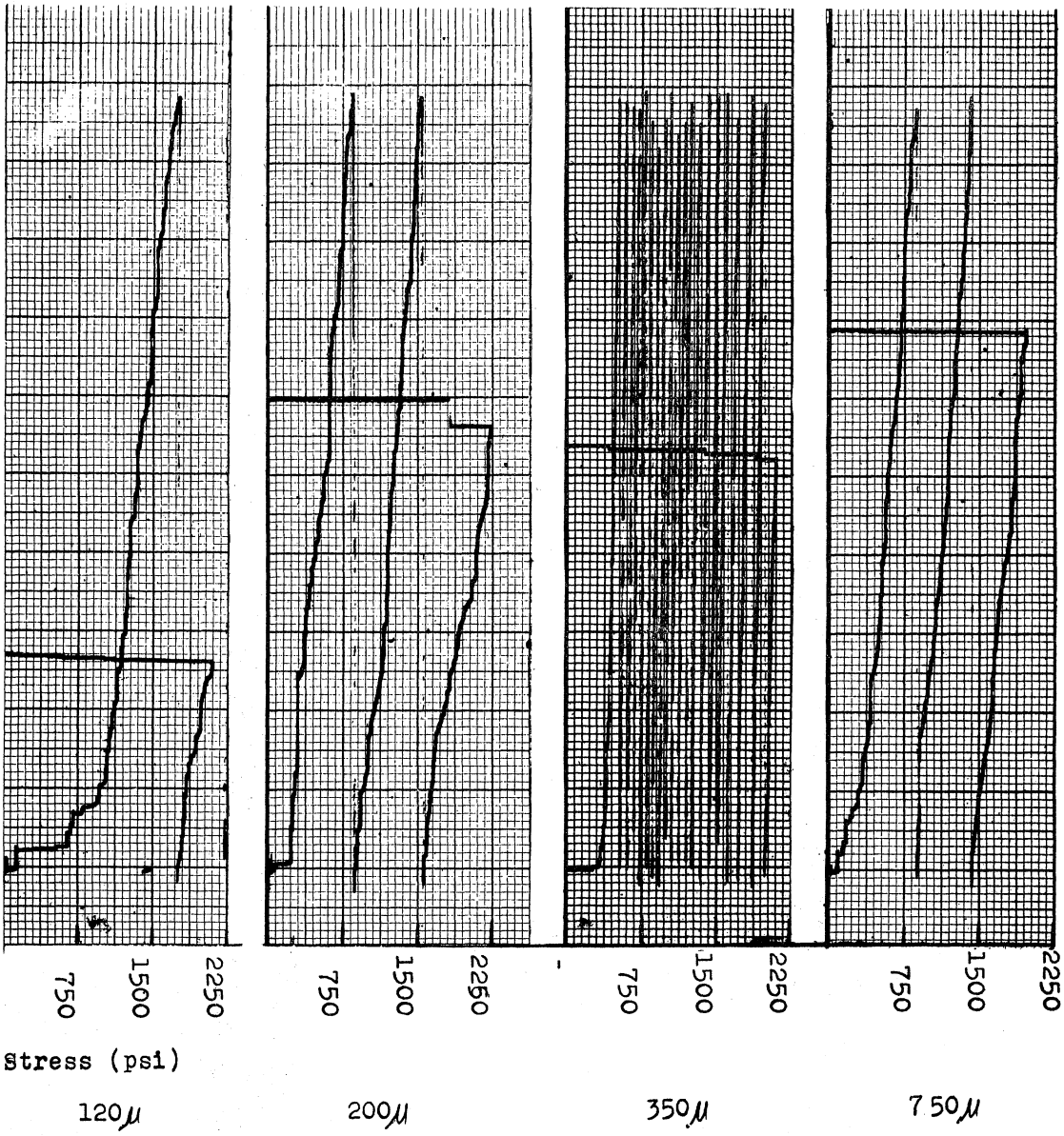

Fig. 3.2 Chart recordings of stress versus number of counts for four different grain sizes. Each $\frac{1}{2}$ inch square on the vertical scale is 100 counts. Trigger level is 0.1v.

Upon unloading, very little emission is observed. Re-loading results in negligible emission until the previously reached load was attained; hence, 99.99% Al displays the Kaiser effect.

3.2.1 0.1 VOLT TRIGGER LEVEL TESTS

A series of tests was run with a 0.1v trigger level setting to determine the effect of grain size on the load emission from 99.99% Al. The results of these tests for a stress of 1500 psi are shown in Fig. (3.3). They show a maximum acoustic emission at a average grain size of about 350 microns. The increase in emission with increasing grain size below 350 microns is attributed to the increase in the slip distance of the dislocations in the individual grains of the material. The decrease above 350 microns is attributed to the decrease in the number of grain boundary sources of dislocation multiplication with the decreasing grain boundary area.

Figure 3.4a shows the variation of cumulative load emission ΣLE with applied tensile stress for cold-rolled specimens of 99.99% Al that have been subjected to a "recovery" heat treatment. They have sub-grain sizes of 10μ and 20μ respectively. The average of the behavior of 2 specimens of each type are plotted. Note the diminishing rate of emission as the applied stress increases, resulting in a downward concavity of the plots. Similar plots for 80% and 20% cold rolled specimens, which were recrystallized to give 750μ and 350μ grain sizes respectively, are shown in Figure 3.4b. The shape of these plots is typical of all recrystallized specimens without a sub-grain structure. Figure 3.4b is an average of the data from 3 specimens of each type. Note the differences in the scales for Figures 3.4a and b.

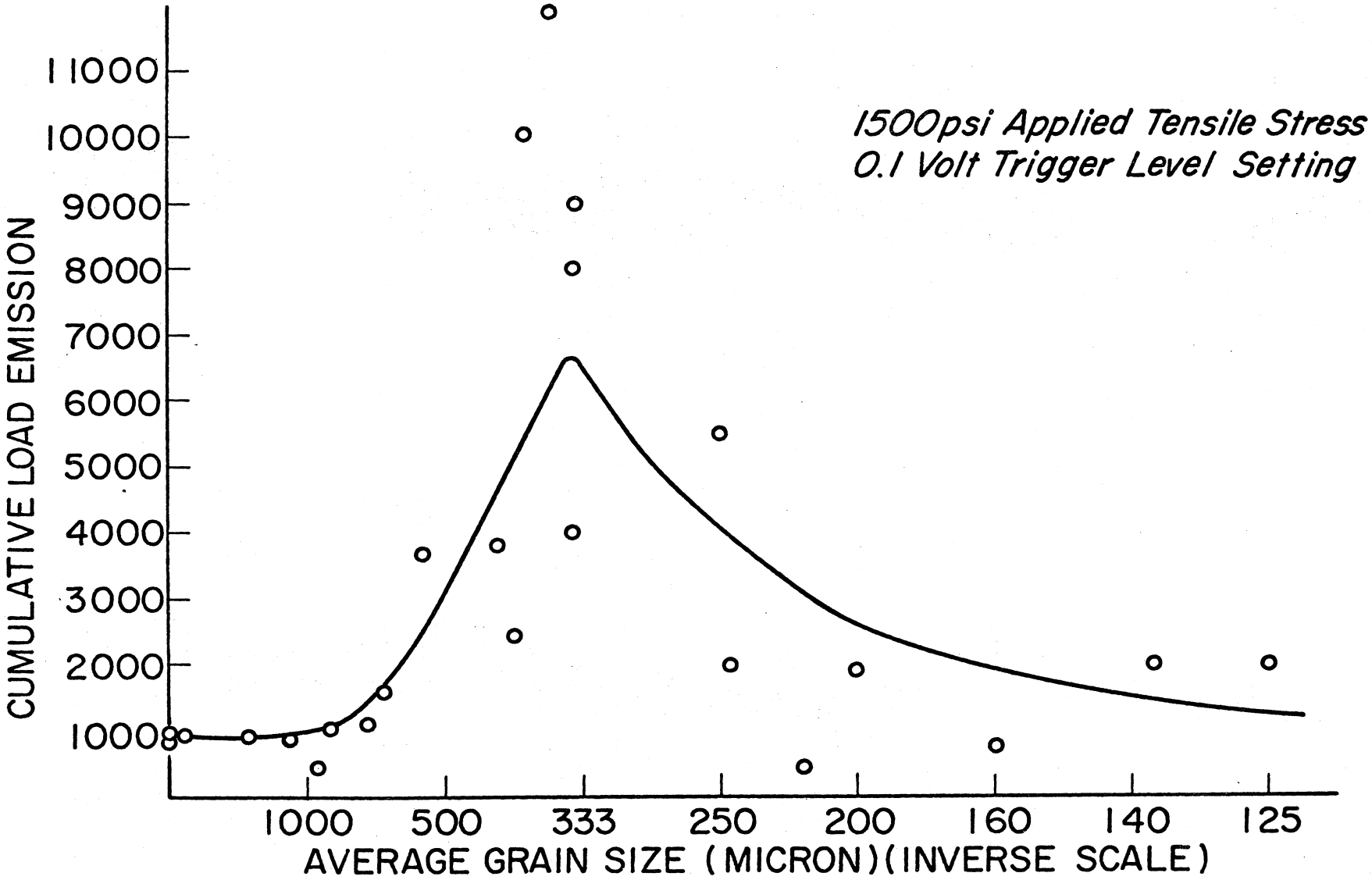

Figure 3.3. Cumulative load emission versus grain size for 99.99% Al in the 120 to 180 kHz bandwidth at 1500psi with a 0.1 volt trigger level setting.

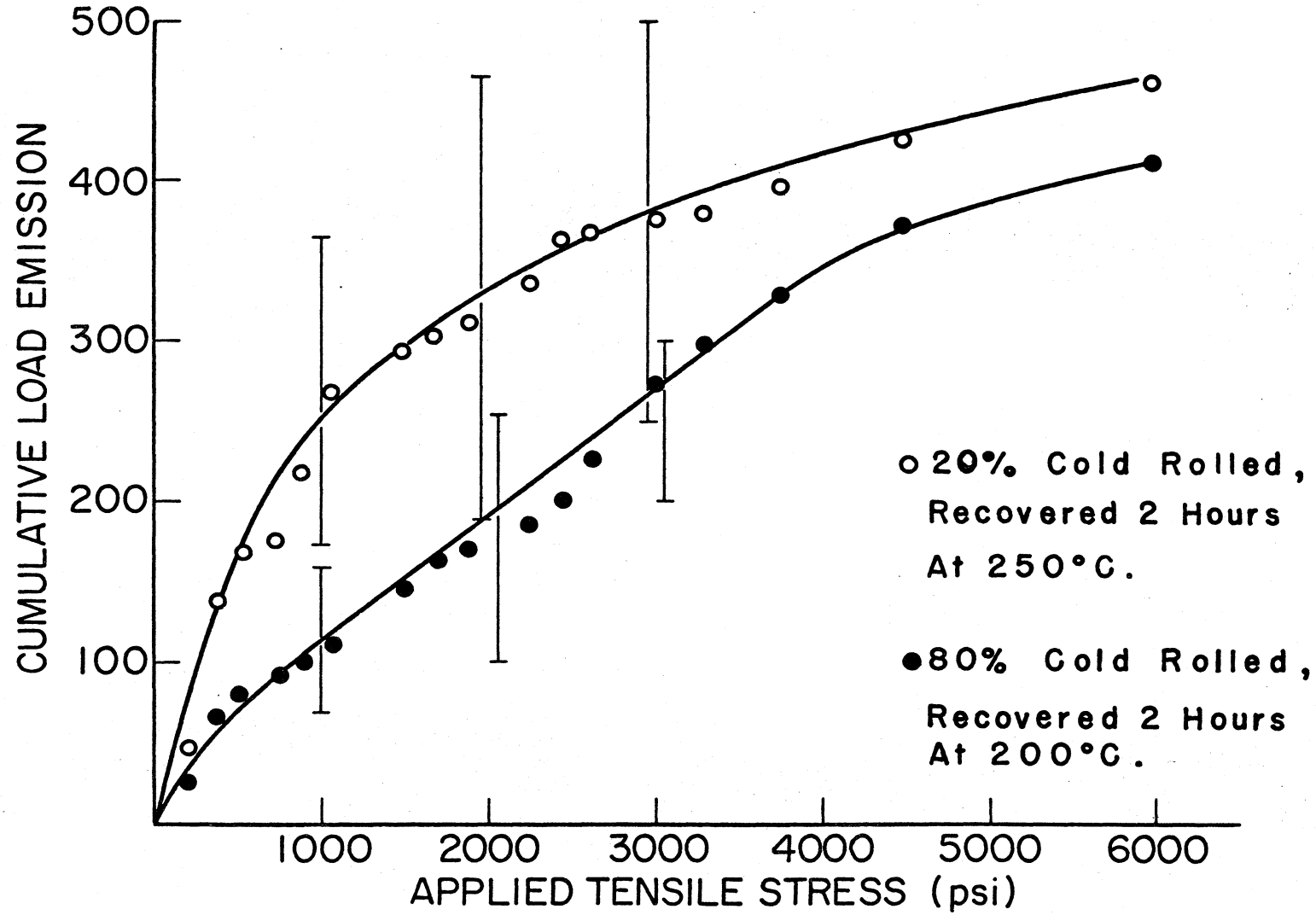

Figure 3.4a Cumulative load emission versus stress for recovered 99.99% Al.

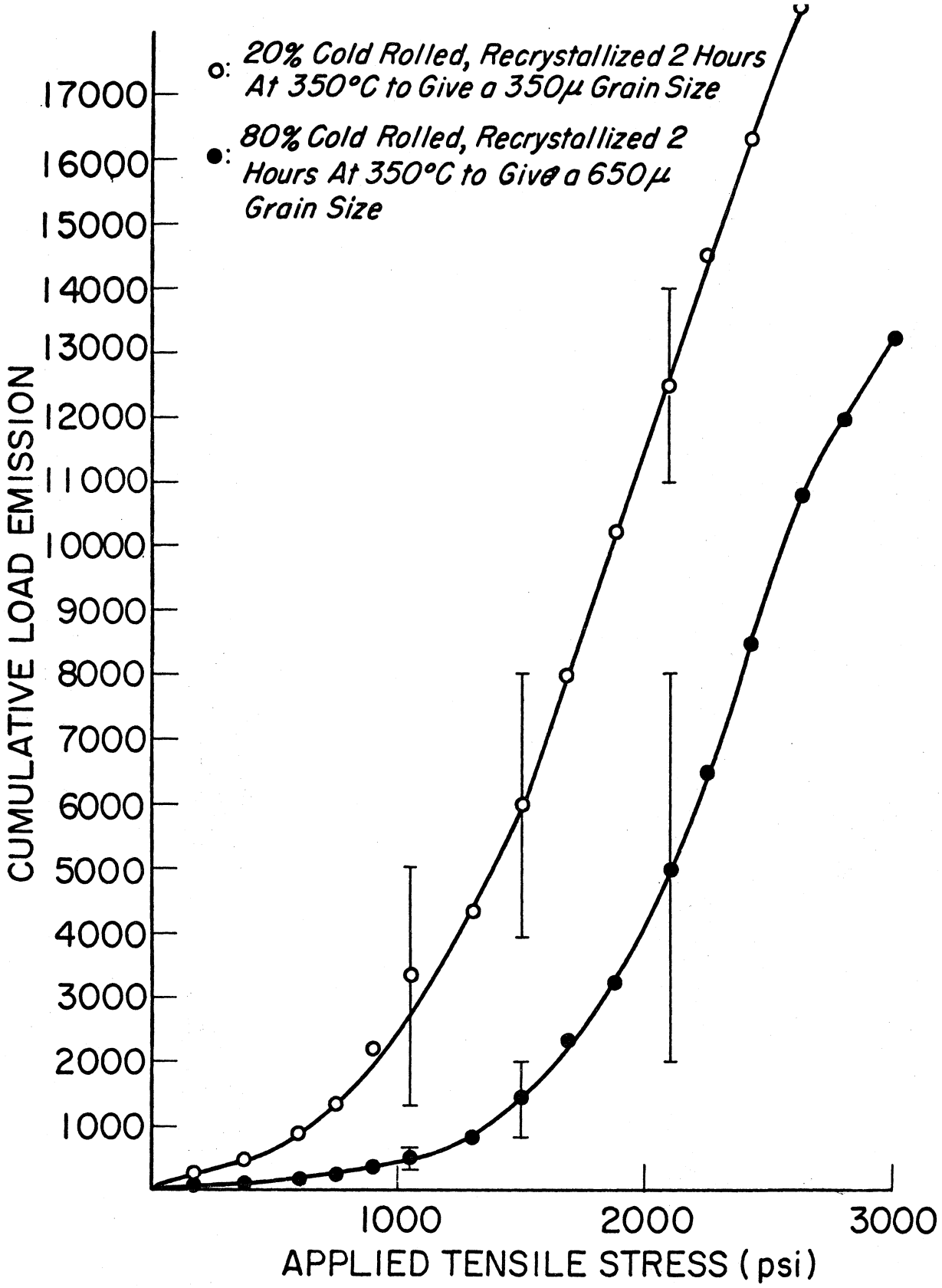

Figure 3.4b. Cumulative load emission versus stress for recrystallized 99.99% Al specimens.

It should be noted that the emission from the large grained specimens is about an order of magnitude greater than that from the small grained structures.

3.2.2 0.2 VOLT TRIGGER LEVEL TESTS

It was hypothesized that the position of the peak in the ΣLE versus grain size curve was a function of the trigger level setting of the acoustic emission counter. To test this hypothesis, a series of tests was run with the trigger level set at 0.2v, rather than 0.1v, thus doubling the minimum transducer displacement required to register a count on the counter.

Sample chart recorder curves for four different grain sizes are displayed in Figure 3.5. The scales are identical to those for the 0.1v trigger level curves. Fig. 3.6 shows ΣLE versus grain size at a stress of 1500 psi. Note that the ΣLE scale for the 0.2v trigger level curves is one-tenth that of the 0.1v trigger level curve shown in Fig. 3.3.

A development of a peak is observed in the 0.2v trigger level tests which differs in two notable ways from the development of the peak in the 0.1v trigger level tests. The first difference is that the peak occurs between 400μ and 450μ grain size. The second difference is that the height of the 0.2v trigger level peak is lower relative to the height of the curve away from the peak, showing a decline in ΣLE with increasing grain size beyond 450μ very nearly proportional to $(D)^{-1}$.

3.2.3 ACOUSTIC EMISSIONS FROM SINGLE CRYSTALS OF 99.99% Al

The crystallographic orientations of the tensile axes of the single crystal specimens were determined by a Laue back-reflection technique. The acoustic emission from two specimens, the tensile axes of which were positively identified, is shown in Figure 3.7. The two specimens are

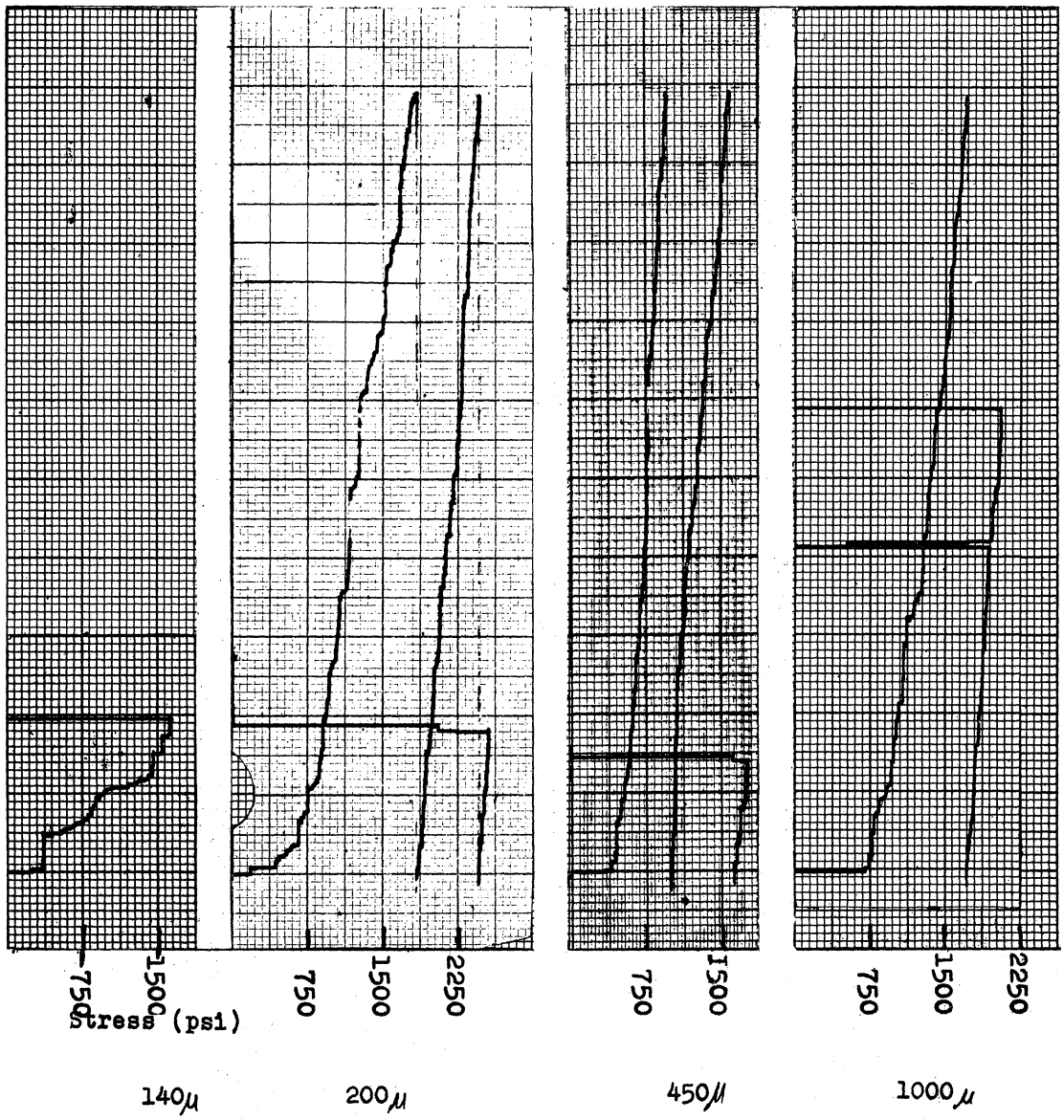

Figure 3.5. Chart recordings of number of counts versus stress for four different grain sizes. Each ½ inch square on the vertical scale is 100 counts. Trigger level is 0.2v.

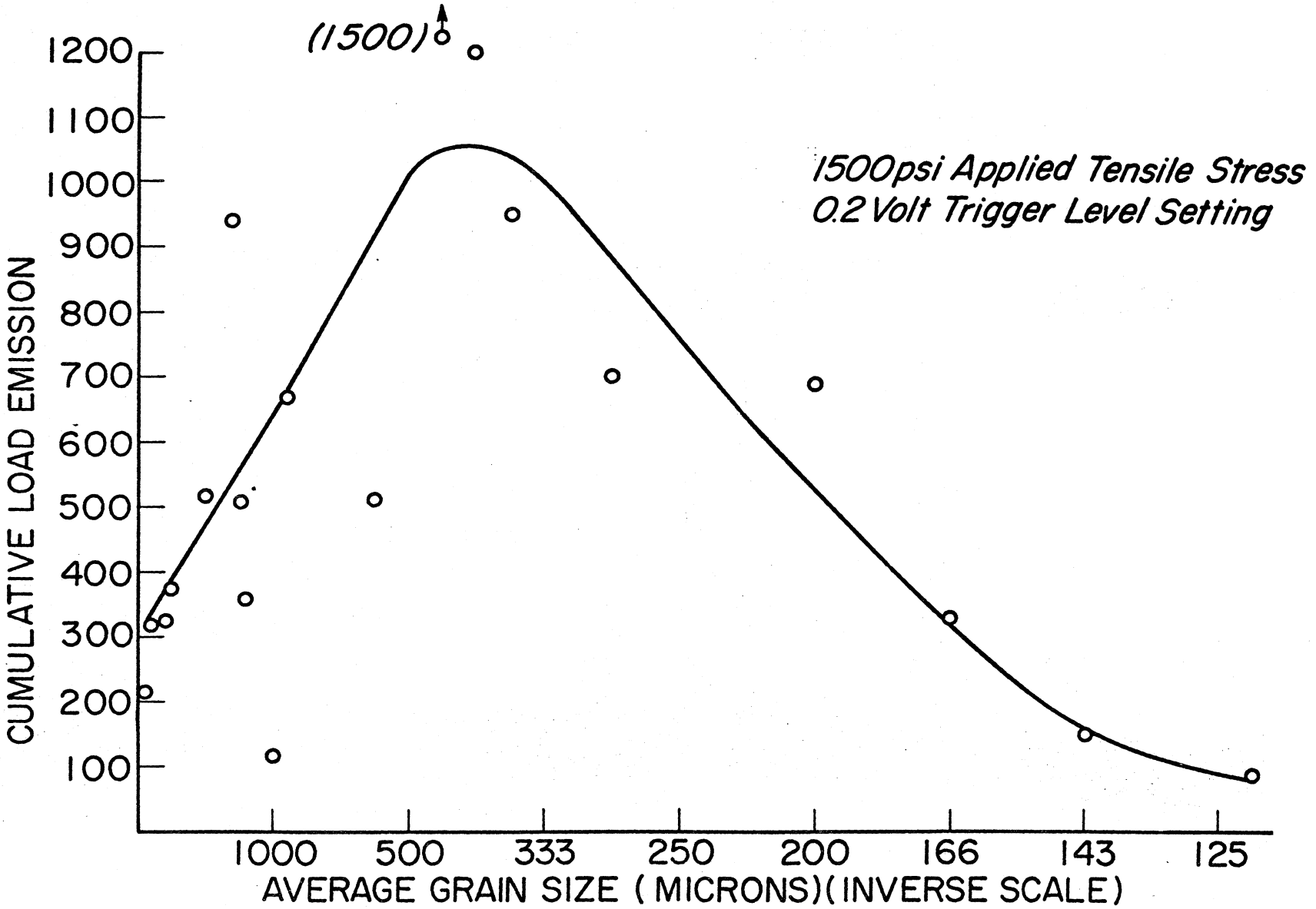

Figure 3.6. Cumulative load emission versus grain size for 99.99% Al in the 120 to 180 kHz bandwidth at 1500psi with a 0.2 volt trigger level setting.

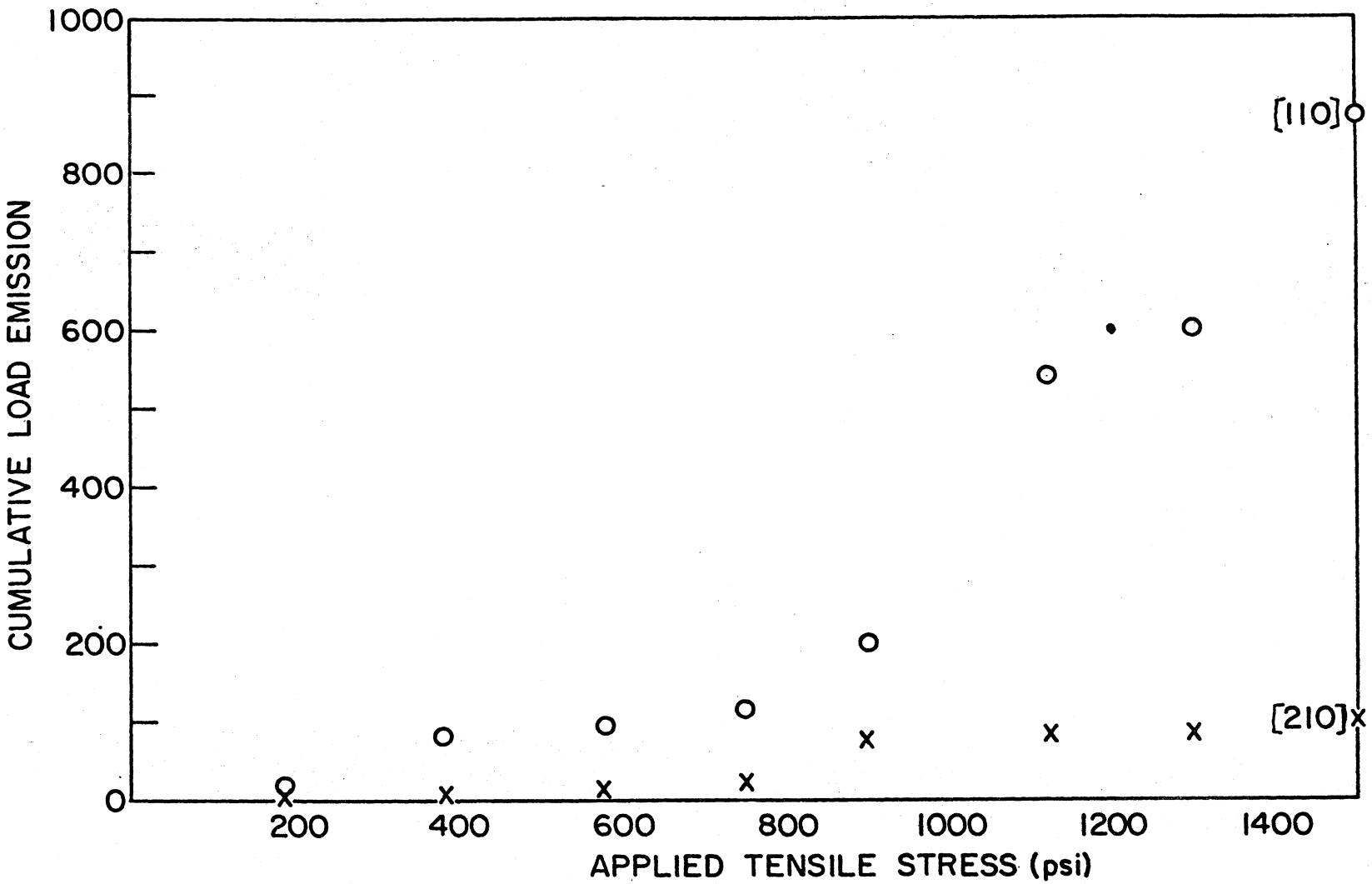

Figure 3.7. Acoustic emissions from single crystals of 99.99% Al.

labelled [210] and [110], after the Miller indices of their respective tensile axes.

The [210] orientation is such that the Schmid factor, also known as the m factor, is a maximum (about 0.49) for a single <110> direction on each of two (111) planes. In the case of the [110] specimen, the m factor is a maximum for two <110> directions in each of two (111) planes. Thus, the [110] specimen, there is a greater possibility of intersecting slip systems at the onset of plastic deformation.

It is interesting that even with the presence of an oxide film, the [110] specimen should give so much more emission than the [210] specimen. Perhaps the emission associated with the surface oxide film[6] is of a lower frequency than 120 kHz, but this is of minor interest here.

3.3 ACOUSTIC EMISSIONS FROM 99.9% Cu

A more limited investigation was conducted on specimens of 99.9% Cu to see whether a grain size effect was present in the cumulative load emission behavior of this metal. Figure 3.8 summarizes the results of this series of tests. A peak, the position of which appeared to be stress dependent, occurred at about 150μ grain size for a 10,500 psi tensile stress level. At 13,500 psi, the peak moved to about a 50μ grain size.

Figure 3.9 shows typical records of tests on 99.9% Cu specimens of a 50μ and 250μ grain size respectively. It can be seen that the acoustic emission activity of the 250μ grain size specimen is much higher once the "high-rate-of-emission" part of the test is reached.

There is a significant difference between the emission behavior of 99.9% Cu and 99.99% Al. Test records show that when obtaining cumulative load emission versus applied stress curves for Cu there is a much larger stress increment between emission bursts in 99.9% Cu than in 99.99% Al. This gives

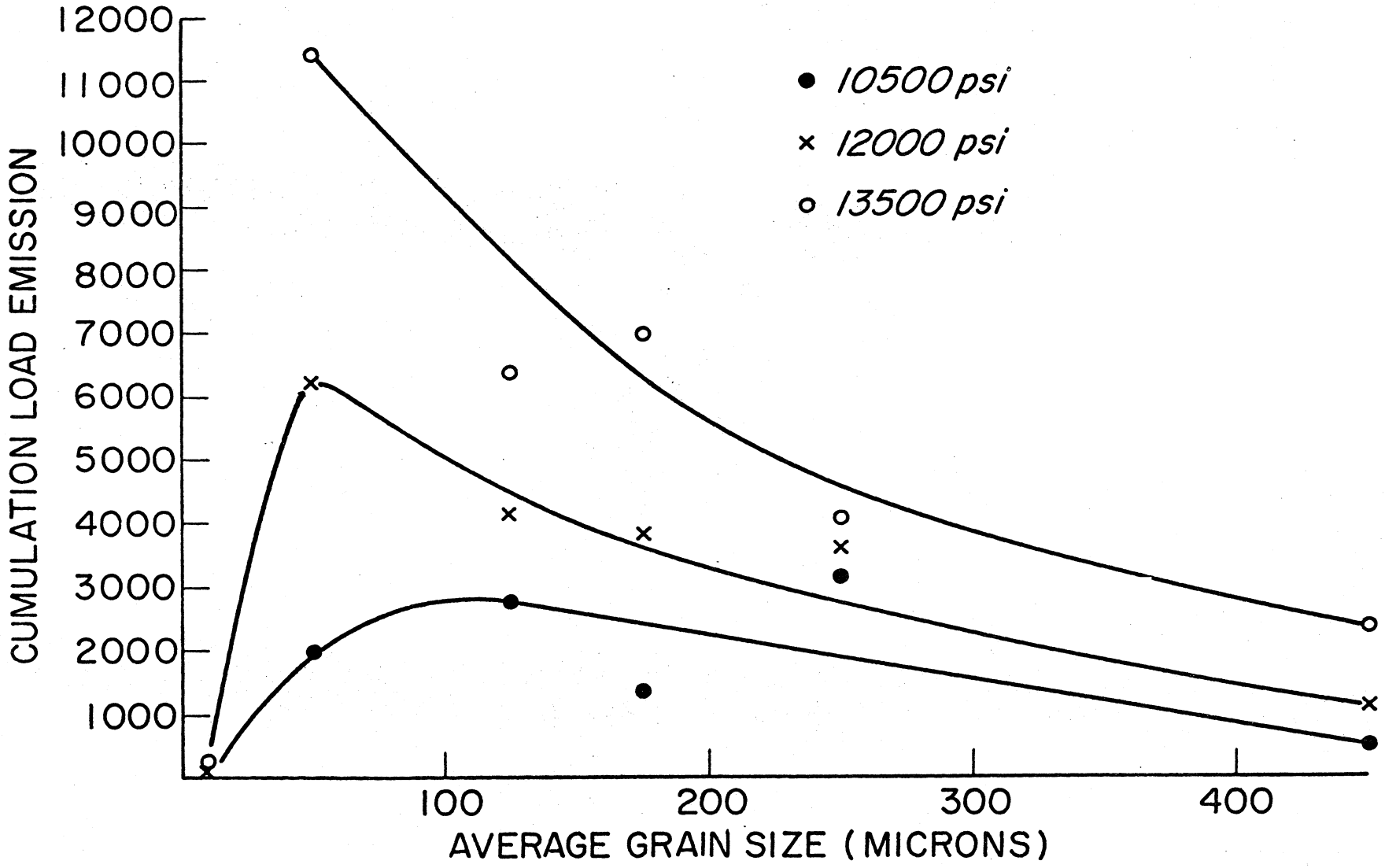

Figure 3.8. Cumulative load emission versus grain size for 99.9% Cu.

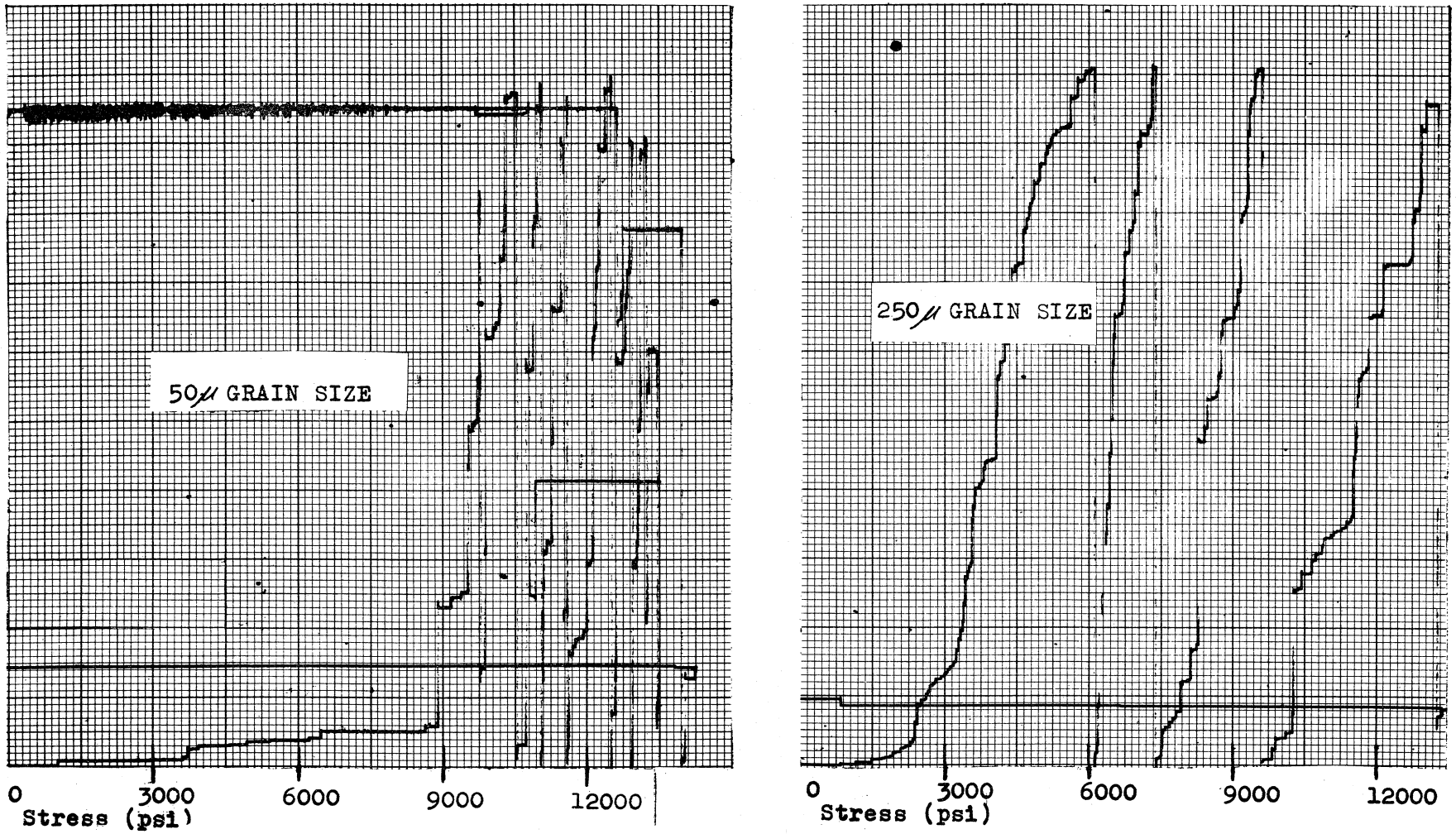

Figure 3.9. ΣLE versus applied tensile stress for 99.9% Cu.

the cumulative load emission curves for 99.9% Cu a characteristic "stepped" appearance.

The emission from both the Cu and the Al occurs in successive groups of bursts. The magnitude of each burst in Cu is large at the beginning of a group, with the signal height declining almost linearly with time. The linear decline in magnitude is in contrast to a fairly uniform magnitude which is seen in groups of bursts from 99.99% Al. The bursts from 99.9% Cu are 5 to 10 microseconds apart, and a typical group of 20 to 40 bursts lasts about 200 microseconds, compared to 400 or 500 microseconds for 99.99% Al. This group-of-bursts quality probably results from a situation in the grains of the metal in which a localized slip event occurs, relaxing stresses in a region of the specimen. This highly local relaxation of stresses triggers other slip events in neighboring regions, resulting in a series of microstrain events occurring in a very short time interval, and within a small volume of the specimen. Stress concentrations resulting from dislocation pile-ups associated with the microstrain event may also play a role in the triggering of a series of events.

3.4 120 TO 180 kHz ACOUSTIC EMISSIONS FROM 2024 Al SPECIMENS

A series of tests, similar to those performed by Agarwal[7] in the 2 to 20 kHz bandwidth, was run on specimens of Alcoa 2024 Al. Comparatively large activity was detected from specimens which were tested within 2 minutes after being quenched from a 530°C solution treatment, as is shown in Figure 3.10. From Figure 3.11 it is seen that very little emission activity is detected from specimens that were solution treated, quenched, and aged for 24 hours at room temperature. An intermediate amount of emission is observed in specimens which were allowed to overage at 315°C. The Rockwell E hardness of the quenched, aged, and overaged specimens are 83, 102, and 77 respectively.

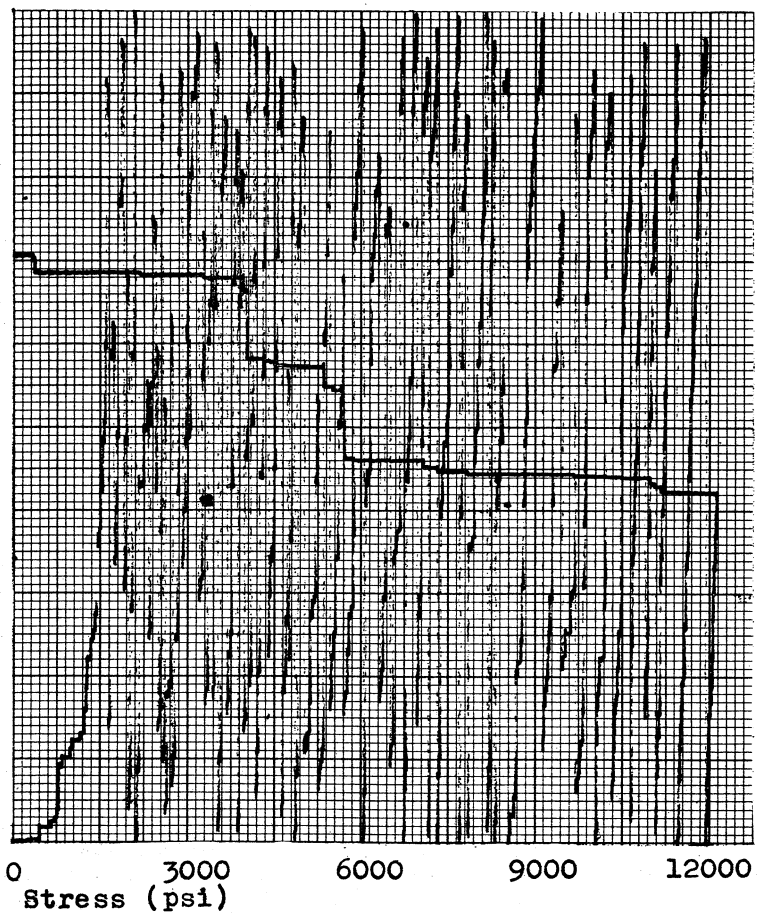

Figure 3.10. ΣLE vs. stress for 2024 Al, solution treated, quenched, and tested within 2 minutes.

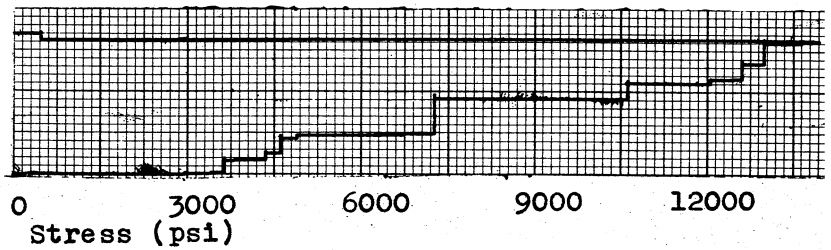

Figure 3.11. ΣLE vs. stress for 2024 Al, solution treated, quenched, and aged for 24 hours at room temperature.

4.0 DISCUSSION OF RESULTS

4.1 MICROSTRAIN RANGE

It is possible to relate the width f of an activated Frank-Read dislocation source with the length L of the pile-up produced by it, and the number of dislocations which it emits. This has been shown[15] for the specimens used in this investigation to be

$$L^3 = \frac{fx2x10^4}{\pi}, \qquad (4.1)$$

where L and f are expressed in microns (μ). The activation shear stress σ_{act} for a given source width is known, and hence Eq. (4.1) gives the minimum slip distance required to produce a detectable acoustic emission. Table 4.1 shows the calculated values of L, σ_{act}, and N for a range of values of the source width, where N is the nbmber of dislocations produced in a pile-up before the resulting back stress shuts the source off.

From dislocation etch pit studies a reasonable estimate of typical source widths in an annealed specimen is between 1μ and 10μ for all grain sizes. This estimate is based on the assumption that the average dislocation spacing corresponds to the distance between pinning points on a dislocation line. Table 4.1 shows that the shear stress required to activate such sources would vary from 1.0 $^{kg}/_{mm^2}$ for f = 1 to 0.1 $^{kg}/_{mm^2}$ for f = 10 . For grain sizes larger than about 130μ, any such source which sweeps across an entire grain should be detectable.

The first acoustic emission activity, consisting of a few counts, is observed to begin at about a 0.1 $^{kg}/_{mm^2}$ (roughly 150 psi) tensile stress. There appears to be no systematic variation in the number of counts versus grain size until a tensile stress of about 0.4 $^{kg}/_{mm^2}$ (600 psi) is reached.

TABLE 4.1

THE ACTIVATION SHEAR STRESS AND REQUIRED SLIP DISTANCE FOR A RANGE OF DISLOCATION SOURCE WIDTHS

f (microns)	σ_{act} (kg/mm^2)	L (microns)	N
0.1	8.6	14	170
1.0	.86	30	37
10	.086	65	8
100	.0086	140	2

The small number of counts detected at a 0.1 volt trigger level at tensile stresses below 0.4 $^{kg}/_{mm^2}$ suggests that the typical microstrain events that occur during the microstrain regime are not characterized by the activation of Frank-Read type sources. Some sources may have been activated, as counts were registered, but the bulk of the microstrain was probably the result of the relatively stable movement of mobile or loosely pinned dislocation segments. Such events would most likely not involve a large enough number of dislocations moving far enough simultaneously to produce a detectable emission. Further consideration will be given in Section 4.2 as to whether or not dislocation unpinning is likely to result in detectable acoustic emissions in the macrostrain regime.

Increasing the counter trigger level to 0.2 volt showed a total lack of emissions in the microstrain regime. This suggests that the maximum slip distance associated with an activated Frank-Read source is not controlled by the grain size, but is limited by the initial dislocation network. If the grain size did control the slip distance, some of the events should have been detectable when the trigger level setting was 0.2 volts.

Stress-strain data obtained during the investigation reveals that the microstrain regime ends at a tensile strain of about 500×10^{-6} for all grain sizes. At this tensile strain the parabolic characteristics of the stress-strain curves give way to an "easy glide" type of curve. The effect that the grain size is observed to have on the stress-strain behavior during microstrain is far less than a third power variation with the average grain diameter as suggested by a model proposed by Thomas and Averbach [16]. The grain size is probably being partially masked by variations in the dislocation density and distribution in specimens. It may be the case that the grain size acts as an upper limit to the distance that a mobile dislocation segment may

move, but it does not influence the length of pile-ups formed during microstrain, nor does it affect the typical distance which a mobile segment moves.

The acoustic emission observations and the stress-strain observations suggest that during microstrain in 99.99% Al the glide distance is not defined by the grain size, at least for grain sizes larger than 100μ. Rather it appears that interactions between moving dislocations and forest dislocations provide the most important strengthening mechanism.

The first dislocation sources activated are probably in the most thinly populated regions of the Frank network. It is in such regions that the longest free dislocation segments occur. As the dislocations produced by the source advance, they run into the more densely populated regions of the Frank network. The strongest interaction between the moving dislocations and the forest dislocations arises from the formation of attractive junctions along some length of dislocation line. The shear stress required to drive a moving dislocation through a network of average spacing ℓ_{min} is[8]

$$\sigma = \frac{G\,b}{3\,\ell_{min}}. \qquad (4.2)$$

Using 1μ as an estimate of ℓ_{min}, and setting f, in Eq. (4.1) equal to 10μ, it is easily seen that the stress which activates the first dislocation sources is not sufficient to advance the resultant dislocations produced through the denser regions of the Frank network. Further microstrain requires the application of additional stress. The additional stress may activate new sources, possibly with the help of stress concentrations ahead of the advancing dislocations. Eventually the applied stress becomes sufficient to drive the mobile dislocations through the densest portion of the Frank

network. Dislocations then begin to reach the grain boundaries in large numbers, and to form pile-ups.

When dislocation pile-ups were observed at the grain boundaries, they were rarely seen to exceed 100μ in length. Often dense "crowds" of dislocation etch pits were observed at the grain boundaries. Such formations may have originally been pile-ups that underwent a blunting process. Blunting occurs when the dislocations near the head of a pile-up cross-slip or climb out of the glide plane of the pile-up. Since both cross-slip and climb are thermally activated processes, dislocation pile-ups must have existed for some time before blunting occurred. Hence, the pile-ups were able to make themselves felt as stress concentrators. Eventually the local stress concentration ahead of a dislocation pile-up held up by a grain boundary becomes high enough to initiate dislocation sources in the neighboring grain. This generally marks the beginning of macrostrain in the specimen.

The acoustic emission results thus lead to the following conclusions regarding microstrain in 99.99% Al.

1. The acoustic emission results suggest that some long dislocation segments may act as Frank-Read sources to give the detected emissions. The dislocations from these sources sweep out a slip area which is determined mostly by the initial dislocation density and distribution. The total lack of counts registered during microstrain in the 0.2 volt trigger level tests indicates that this slip area must be considerably less than the cross-sectional area of a grain, and probably does not vary much with grain size.
2. The comparatively small number of counts registered during microstrain suggests that a considerable portion of the microstrain results from the movement of relatively mobile dislocations, and not necessarily from the activation of dislocation sources. This is similar to the

microstrain processes envisioned by Bilello and Metzger[1] to occur in copper.

4.2 ACOUSTIC EMISSION BEHAVIOR IN THE MACROSTRAIN RANGE, AND THE MECHANISMS PRODUCING IT

At tensile stresses of 0.4 to 0.5 $^{kg}/_{mm^2}$ (600 to 750 psi), specimens with grain sizes larger than 200μ appear to have entered the macrostrain range. Macrostrain is characterized by a nearly flat appearance of the stress-strain curve, with the slope varying slightly with grain size. Acoustic emission data show a rather sudden increase in the rate of emission even before the macrostrain regime is reached, at a tensile stress of about 450 psi for all grain sizes larger than 200μ. Once this high-rate-of-emission regime is reached, the cumulative load emission ΣLE is approximately proportional to the applied stress. This implies that the rate of emission is approximately proportional to the plastic elongation, at least up to elongations of about 2 percent. Fig. 3.3 shows the strong effect that the grain size has on this proportionality factor in the macrostrain regime. These observations provide some clues as to how deformation--at least the deformation detected by the acoustic emission transducer--proceeds during macrostrain.

There are two phenomena that might give rise to the emissions detected during macrostrain. One is the widespread unpinning and coordinated movement of dislocations, and the other is the activation of dislocation sources.

Consider first the unpinning and coordinated movement of dislocations. If this is the controlling source of emissions it must explain both the uniform rate of emission with strain, and the observed effect grain size has on the cumulative load emission ΣLE behavior. Suppose that dislocations, upon being unpinned, are able to move across an entire grain and are stopped

by grain boundaries. Such unpinning events may be envisioned to occur as an "avalanche" of dislocations spreading across a grain. The magnitude of such events should be roughly proportional to (grain size)^3, the number of dislocations involved being proportional to the grain size, and the slip area being proportional to (grain size)^2. This would predict that the total number of events activated at a particular value of plastic strain be proportional to (grain size)$^{-3}$. Plots of ΣLE versus grain size on the descending side of the peak, using some value of plastic strain rather than an applied stress level as the constant parameter show that ΣLE is roughly proportional to (grain size)$^{-2}$. This alone doesn't necessarily disqualify the model of unpinned dislocations forming avalanches that are stopped by grain boundaries, but the following considerations cast doubt on its validity.

The initial dislocation etch pit density of all recrystallized specimens was roughly 10^6 per cm^2. Using the relation

$$\frac{\text{Length of line}}{\text{unit volume}} = 2 \times \frac{\text{number of intersections}}{\text{unit area}}$$

gives $2 \times 10^6 \frac{\text{cm}}{\text{cm}^3}$ as the length of dislocation line per unit volume in a specimen. Assuming that all of the initial dislocations are mobilized and move, on the average, a distance of 1/2 the grain size, the equation

$$\gamma = \frac{vM\, b\, \frac{D}{2}}{v}$$

expresses the maximum shear strain possible from the unpinning, and subsequent movement of initial dislocations alone. The volume of the specimen is v, M is the length of dislocation line per unit volume.

The maximum elongation possible by this mechanism is about 0.15%. Hence, if unpinning is the major cause of the emissions detected, it requires that a continous generation of dislocations occur concurrently. The assumption that the activation of dislocation sources is not the major cause of emissions further requires that the freshly generated dislocations undergo successive pinning-unpinning processes, and some possible secondary dislocation motion associated with them that give rise to the emissions.

So far, the unpinning model can adequately explain the observed uniform rate of emission with strain, but it is necessary to acknowledge the possibility of dislocation generation in order to account for the amount of strain over which uniform emission occurs. Further, it is necessary to justify the assumption that the activation of these sources is not the major cause of the dtected emissions. Intragranular obstacles provide opportunities for successive pinning and unpinning of the dislocations generated by the sources, and these unpinning actions cause most of the emission. The requirement that such intragranular obstacles be dominant implies that the grain boundaries must be masked as sources of emission behavior of a specimen. This is certainly not the case.

From these arguments it may be concluded that the major cause of the detected emissions, at least for a certain range of grain sizes, is not the unpinning of dislocations. This suggests that the activation of dislocation sources be considered as a mechanism leading to the generation of acoustic emissions.

Without going into a detailed discussion, source activation may be used as a model to explain the observed uniform rate of emission with increased applied stress. Each increment of applied stress activates a uniform additional number of dislocation sources. As an incidental point,

this may imply that the distribution of sources is inversely proportional the source width, i.e.

$$\Delta LE \propto \Delta\sigma \Rightarrow \Delta N \propto \frac{1}{f}$$

where ΔN is the number of additional sources activated by the stress increment $\Delta\sigma$, and f is the average width of those sources activated as the stress increases from σ to $\sigma + \Delta\sigma$. Such a statement is complicated, however, by the possibility that new sources are created as strain proceeds.

The final question to be answered is "can the source activation model explain the observed variation in the rate of emission with grain size?". Assume first that there exists a grain size independent distribution of dislocation sources in a specimen. At a given level of applied stress, all sources down to a certain width should have been activated. Examination of Table 4.1 indicates however, that the grain size is not likely to control the detectability of sources which are smaller than 10μ. Such a model cannot easily explain the observed ΣLE versus grain size variation.

As a final attempt to develop a satisfactory model involving the activation of dislocation sources, attention is to be focused on the grain boundaries themselves. During the course of the investigation studies have been made of the changes in the appearence of slip lines in the microstructure of the 99.99% Al as the applied stress was increased from 300 psi to 900 psi in increments of 150 psi. The results of this effort indicate that slip in one grain activates slip on secondary systems in adjacent grains. These observations, combined with the observation that the grain size effect on the ΣLE versus grain size curve began to emerge at tensile stresses of about 600 psi motivate the proposal that the major cause of the emissions detected

is the activation of dislocation sources near the grain boundaries when slip is propagated from one grain to its neighbor. This is essentially the intergranular slip model proposed by Cottrell[9], and it will now be applied to the acoustic emission observations as a possible explanation of the ΣLE versus grain size variation.

4.3 THEORY OF THE SHAPE OF THE ΣLE VERSUS GRAIN SIZE CURVE

Intergranular slip occurs when plastic strain is propagated, by some mechanism, through a grain boundary. Typically, intergranular slip does not begin simultaneously throughout the entire specimen, but starts at a few localized regions and becomes more and more predominant as deformation proceeds.

Consider a typical grain boundary in a recrystallized specimen. As was discussed by Li (Ref. 2), Cottrell envisions the propagation of slip across a grain boundary to occur when the resolved shear stress at the head of a dislocation pile-up held up by the grain boundary reaches a critical value σ_o. A suggested mechanism was the activation of a Frank-Read source in the adjacent grain, near the grain boundary. If there are N dislocations in the pile-up, an applied shear stress σ exerts a stress $N\sigma$ on the grain boundary. The number of edge dislocations in a double pile-up is given by[10]

$$N = \frac{2(1-\nu)\sigma L}{Gb} \tag{4.3}$$

where L, in this case, is the distance from the source to the leading dislocation of the pile-up. If L is assumed to be equal to one half the average grain diameter D, the stress applied by the pile-up on the grain boundary may be taken as

$$N\sigma = \frac{2D\sigma^2(1-\nu)}{2Gb} \qquad (4.4)$$

The validity of taking L as $\frac{1}{2}D$ is questionable, particularly since the length of the dislocation pile-ups which were observed at a 0.8 $^{kg}/_{mm^2}$ tensile stress was not seen to be controlled by the grain size. From a stress concentration standpoint, the effective length of a dislocation pile-up may have an upper limit determined by the surrounding dislocation network density[11]. The local stress induced by the pile-up may activate secondary sources in the network. These secondary sources may interact with the pile-up dislocations, effectively dividing a large pile-up into a series of shorter ones. Also Eq. (4.4) takes no account of the effect of blunting which, based on etch pit studies and the relative ease of cross slip in aluminum probably occurs.

The typical acoustic emission data of Figure 3.2 indicate that up to a 200μ grain size, a lower applied stress is needed to initiate the high-rate-of-emission as grain size increases. For grain sizes larger than 200μ, little consistent effect upon the stress level at which high-rate-of-emission begins is observed. From the slip line studies, this stress level corresponds fairly well with the stress level at which slip seems to begin to propagate across grain boundaries. Hence, it may be proposed that up to about 200μ, the grain size serves as an upper limit to the effective pile-up length. Beyond 200μ, the length of a typical pile-up is not controlled by the grain size.

If the length of a pile-up is L, and x is the distance ahead of the pile-up on its glide plane, the local shear stress at x is approximately given by [11]

$$\sigma_x \simeq \sigma[1 + (\frac{L}{x})^{1/2}] \qquad (4.5)$$

where σ_x is the local shear stress, and σ is the applied shear stress. Eq. (4.5) is valid for $x \ll L$, but greater than the distance between the two leading dislocations. For $x \gg L$, the local shear stress at x is[11]

$$\sigma_x \simeq \sigma[1 + \frac{L}{2x}]. \qquad (4.6)$$

Applying these equations to grain boundary pile-ups ignores the orientation difference across the grain boundary. An accurate resolved shear stress relationship would require a complete stress tensor analysis coupled with knowledge of the misorientation across the grain boundary. Since both are impractical, Eq. (4.5) and Eq. (4.6) will be applied, bearing in mind the approximations involved. The significance of the above two equations is that the stress concentration due to the presence of a pile-up is long range in nature. Hence, well into the grain adjacent to the one in which the pile-up exists, the local shear stress is considerably higher than the applied shear stress. This factor should aid in the movement of dislocations across the adjacent grain at high velocities.

When the stress field due to the pile-up succeeds in triggering a dislocation source in the adjacent grain, the local stresses on the source are quickly relaxed to a level just below that necessary to operate the source. This quick relaxation of stress is caused by the nearness of the source to the grain boundary. A small increment in applied stress is necessary to cause a further increment of slip across the grain boundary. In effect, a large angle grain boundary is step-wise unstable as a slip obstacle. Figure 4.1 shows a possible sequence of events leading to a

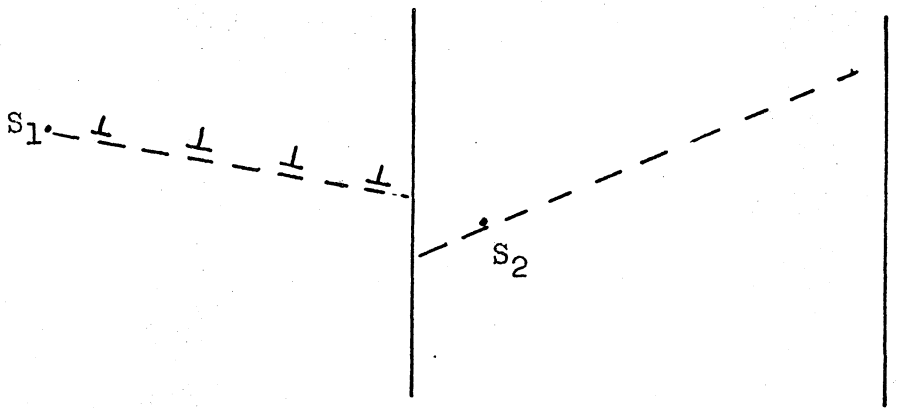

Applied stress activates source S_1, which produces a dislocation pile-up held up by the grain boundary.

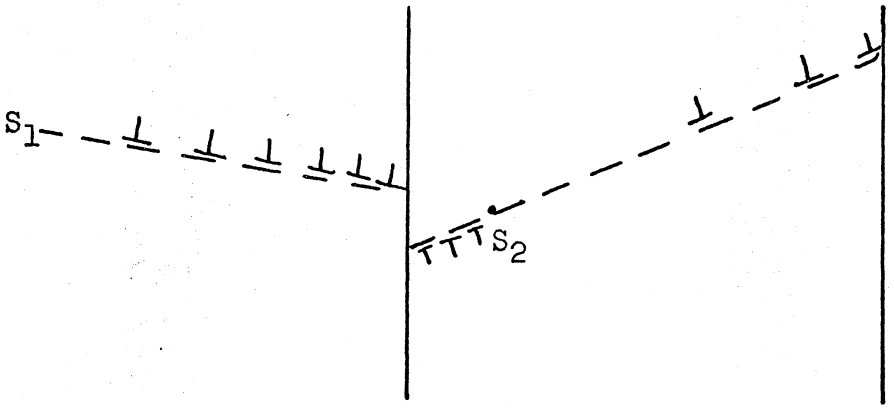

As the pile-up grows under increased stress, it activates the source S_2 in the adjacent grain.

Fig. 4.1. Grain boundary source mecha

grain boundary "breakthrough". The proximity of the source S_2 to the grain boundary limits the number of dislocations it may emit in an unstable step to just a few, maybe from one to ten.

Suppose that there is a grain size independent density of grain boundary sources, such as S_2, per unit grain boundary surface area. Assume all that the width of these sources is grain size independent. Then, at a given applied stress, the number of these sources which had been activated by local stress concentrations should be proportional to the total grain boundary surface area, which in turn is proportional to D^{-1}, where D is the average grain diameter. This, of course, is assuming that the density of grain boundary sources, and not the density of dislocation pile-ups which reach the grain boundaries, is the parameter controlling the number of grain boundary sources that are activated.

If the grain boundary model can now adequately explain the observed acoustic emission behavior, in particular the ΣLE versus grain size variation, it would be reasonable to state that it is the major cause of the acoustic emissions detected in polycrystalline Al specimens. It has been shown that the number of grain boundary sources activated should be proportional to the grain boundary surface area, hence proportional to D^{-1}. If N is the number of dislocations that take part in a slip event which produces acoustic emission and "a" is the minimum slip area necessary to produce an acoustic emission, and if N equal to ten is taken as an upper limit to the number of dislocations produced in a single burst by one of the grain boundary sources, the minimum slip area that can yield a detectable emission from such a source is $10{,}000\mu^2$, and the corresponding grain diameter is about 320μ. Thus, a plot of the likelihood of detecting the activation of a grain boundary source, when the trigger level setting is 0.1 volt, should

be very small for grain sizes smaller than 100 μ, increase continuously as the grain size increases from 100 μ to 320 μ, and undergo no further increase as the grain size increases beyond about 320 . Between 100 μ and 320 μ, the rate at which the likelihood of detection increases with grain size is difficult to specify, being complicated by three factors:

1. there is certainly scatter in the grain size within a given specimen;
2. the actual slip area depends on the way in which the slip plane cuts across the grain;
3. dislocation obstacles such as Lomer-Cottrell barriers, impurities, and forest dislocations would result in a variation in the actual slip area swept out in a single step, with (grain size)^2 as an upper limit.

A plot of the total number of grain boundary source events detected by the transducer should be a plot of the product of the number of grain boundary sources activated (proportional to $\frac{1}{D}$) times the likelihood of detecting a source. Figure 4.2 shows this function graphically. Notice that a peak is produced at a 320_{μ} grain size.

At stresses on the order of 0.8 $^{kg}/_{mm^2}$ to 1 $^{kg}/_{mm^2}$, some intragranular dislocation sources should be detectable, in addition to the grain boundary associated sources. These additional detectable events may be easily accounted for by considering Table 4.1. For grain sizes larger than 130_{μ}, the cumulative activity produced by intragranular sources should not vary much with grain size even if the grain size does control the slip distance at stresses on the order of 1 $^{kg}/_{mm^2}$. Hence, a constant level of activity may be added to the dashed curve of Figure 4.2a to give the total number of events one would expect to detect during a 0.1 volt trigger level test. This total number is represented by the solid curve of Figure 4.2a.

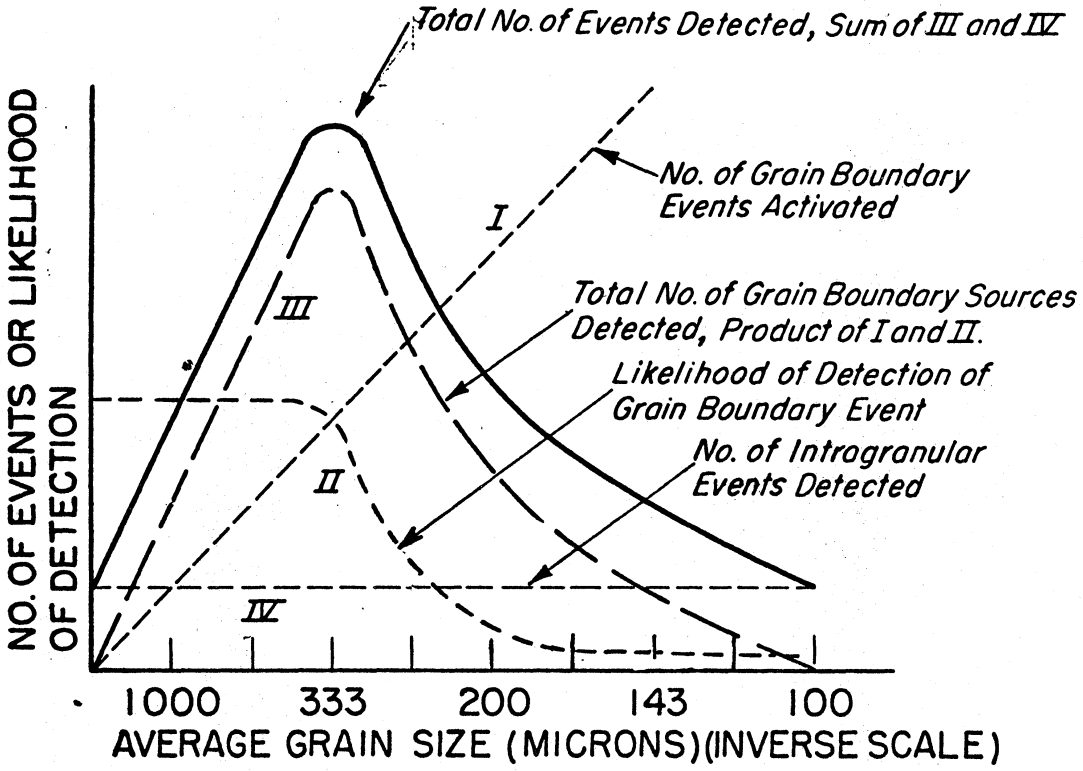

Figure 4.2a. Graphical representation of acoustic emission behavior model based on the activation of grain boundary sources. 0.1 volt trigger level.

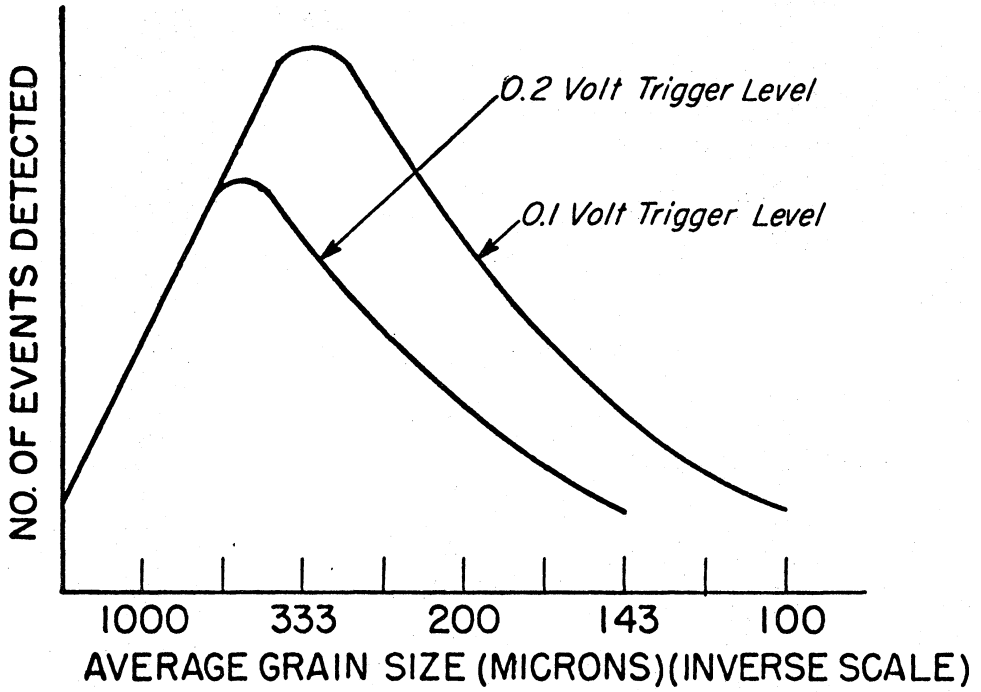

Figure 4.2b. The effect of changing the trigger level setting.

The behavior shown in Fig. 3.3 is fairly well described by the solid curve of Figure 4.2a. The theory developed accurately predicts the position of the peak, and the constant level of ΣLE for increasing grain sizes beyond about 1000μ.

In Fig. 3.6, the peak in the ΣLE versus grain size curve was observed to be less prominent for the case of the 0.2 volt trigger level test than for the 0.1 volt trigger level tests. Also, the peak occurred at a grain size of 400μ to 500μ in the 0.2 volt trigger level tests.

The shift in the position of the peak for the 0.2v trigger level tests is to be expected for the following reason. In doubling the trigger level, by changing it from 0.1 volt to 0.2 volt, the minimum detectable surface displacement "a" is doubled. If the relationship between the number of moving dislocations and the minimum detectable area, namely,

$$Na = 10^{-7}(\text{meter})^2 \qquad (4.7)$$

is assumed to be valid (ref. 3), then the smallest slip area that can yield a detectable emission from a grain boundary source (set N equal to ten) is $20{,}000\mu^2$, corresponding to a grain size of 141μ. Similarly, the saturation condition (set N equal to one) occurs at a grain size of 451μ, which is larger by a factor of $\sqrt{2}$ than the saturation condition for the case of a 0.1 volt trigger level. Thus, it is to be expected that doubling the trigger level should translate the position of the peak by a factor of $\sqrt{2}$ to a larger grain size. This accurately describes the observed effect of raising the trigger level from 0.1 volt to 0.2 volt.

In view of the approximate nature of the analysis, the observed positions of the peaks in the 0.1 volt and 0.2 volt trigger level curves appear to be in

good agreement with the theory developed.

4.4 ACOUSTIC EMISSIONS FROM 99.99% Al SPECIMENS THAT HAVE BEEN SUBJECTED TO A RECOVERY HEAT TREATMENT

Owing to the nature of sub-grain walls, and the comparatively small slip area available within a sub-grain, the grain boundary source mechanism that was proposed to account for the behavior of the recrystallized specimens is not applicable to the case of the recovered specimens in which sub-grains are present. Any microstrain event which is constrained to within a single sub-grain will be unlikely to result in a detectable acoustic emission. This may be seen by considering Table 4.1, and recalling that the largest sub-grains under consideration are only about 20μ long.

Slip may spread from one sub-grain to the next by three basic mechanisms[2]. Two of them involve the generation of dislocations by the sub-boundary. Dislocation "generation" occurs either by moving unpinned dislocations away from the boundary, or by unpinning pinned dislocations and then moving them away from the boundary. The third basic mechanism is the movement of dislocations from one sub-grain to the next by forcing moving dislocations through the sub-grain wall. This mechanism is modelled by considering the sub-boundary to be a simple tilt boundary.

A characteristic stress σ_o is required to activate each of the three mechanisms. Calculated values of σ_o for each of the three mechanisms are shown in Table 4.2. The calculations are based on the equations proposed by Li[2].

Under certain circumstances it may be possible that σ_o is achieved at the head of a dislocation pile-up. Using one-half the sub-grain size as the pile-up length, the value of the local stress at the head of a pile-up is given by

$$\sigma_{local} = \frac{2(1-\nu)\sigma^2 d}{Gb} = \sigma_o \qquad (4.7)$$

for the case of edge dislocations. Table 4.2 includes values of σ required to achieve the respective σ_o for each sub-boundary "breakthrough" mechanism.

The dislocations of a pile-up are assumed to come from a Frank-Read type source. The source may be in the center of a sub-grain, or it may consist of a segment of unpinned dislocation in a sub-boundary. The minimum source width that may be active under the applied shear stress σ is also included in Table 4.2. The activation of a source to produce a pile-up is considered to be a practical impossibility if f is larger than about one-half d.

Table 4.2 suggests that as the applied stress increases, the first microstrain events that occur are the movement of unpinned or loosely pinned dislocations from the sub-grain walls. This undoubtedly occurs without the aid of dislocation pile-ups. The stress-strain data indicate that the cumulative strain resulting from the movement of these dislocations is quite small. The initial comparatively high rate of emission from the recovered specimens is probably the result of the movement of such loosely

TABLE 4.2

REQUIRED CONDITIONS FOR SUB-BOUNDARY BREAKTHROUGH

Mechanism / Requirements		Movement of Dislocations From an Unpinned Sub-boundary	Movement of Dislocations From a Partially Pinned Sub-boundary			Dislocations Forced Through a Simple Tilt Boundary		
			n=10	n=5	n=1	θ=10°	θ=5°	θ=1°
	σ_o	0.1	2	4	20	200	100	20
For 10μ Sub-grain	σ	.074	0.35	0.5	1.2	3.5	2.5	1.2
	f	12	2.4	1.8	0.7	0.26	0.34	0.7
For 20μ Sub-grain	σ	.05	0.25	0.35	0.8	2.5	1.8	0.8
	f	18	3.4	2.6	1.1	0.34	0.48	1.1

θ: Angle of misorientation across a tilt boundary.

n: Ratio of the number of unpinned dislocations to pinned dislocations.

σ: Applied shear stress (kg/mm^2) required to activate a particular mechanism.

σ_o: Local shear stress (kg/mm^2) required to activate a particular mechanism.

f: Width of the source (microns) that forms the pile-up that may aid in "breakthrough".

pinned dislocations from the sub-boundary walls. To produce a detectable emission by this mechanism, there must either be a coordinated unpinning and movement of dislocations from the sub-boundary walls, or else a general activation of this mechanism throughout the specimen must occasionally give rise to superimposed stress waves. At tensile stresses greater than about 1 $^{kg}/_{mm^2}$, a decline in the rate of emission with increasing stress is observed. This decline is probably the consequence of an exhaustion of the easily unpinned and moved dislocations. Further strain and emission is the result of either more tightly bound dislocations being moved from sub-grain walls, or the breaching of sub-grain walls by the forcing of dislocations through them; both mechanisms are probably aided by the formation of pile-ups.

Since the slip area available within a sub-grain is so small, the likelihood that the formation of a dislocation pile-up will produce a detectable emission is nil. An emission may be produced if, as a consequence of breaking through a sub-boundary, a pile-up is able to sweep out an area large enough to satisfy Eq. (4.7). An "unzipping" type of operation, by which the dislocations of a pile-up may be able to sweep out an area many times larger than that of a single sub-grain, is shown in Figure 4.3.

In step 1 of Figure 4.3, a dislocation pile-up is formed in sub-grain a.). The sub-boundary between a.) and b.) is breached in step 2, and the dislocations spew across sub-grain b.). The sub-boundary between b.) and c.) may be quickly breached if it is of about the same strength as, or weaker than the sub-boundary between a.) and b.); the dislocations are then free to run across sub-grain c.). In step 3, the boundary between sub-grains a.) and c.) is lined by attractive segments of the continuous dislocation loops, and may be quickly breached. This produces the configuration shown in step 4. A continuation of this process through all the sub-grains surrounding a.) may lead to the configuration shown

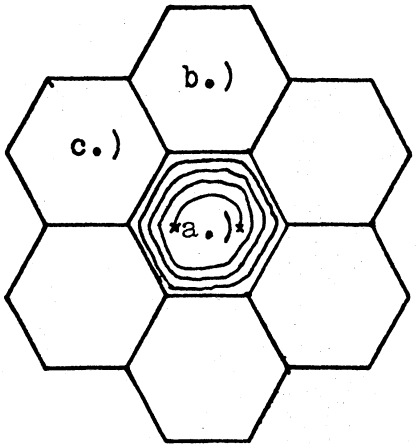

STEP 1

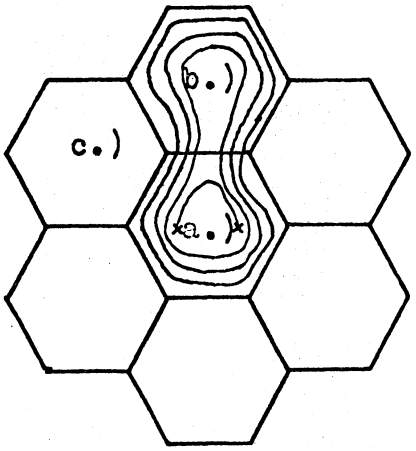

STEP 2

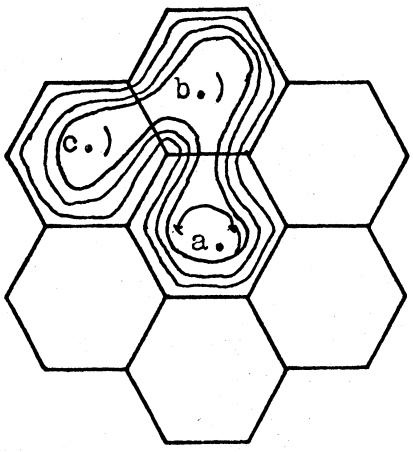

STEP 3

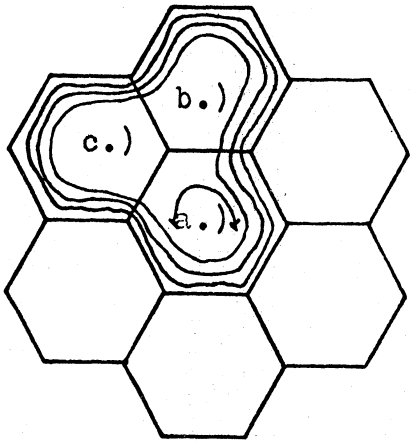

STEP 4

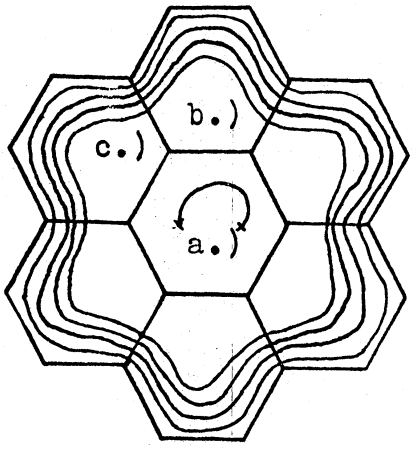

STEP 5

Figure 4.3. Sequential sub-grain boundary breakthroughs.

in step 5. The increase in pile-up length allows the original source to produce more dislocations which may aid in further perpetuating such a process.

Whether such a process as that depicted in Figure 4.3 can occur in an unstable enough manner to produce a detectable emission depends on the nature or the interaction of the sub-boundary walls with moving dislocations. If a great many jogs are formed on the screw components of the loops, the drag stress will quickly rise to such a level that the process will be slowed down. Such jogging interactions may eventually result in dipole formation, and could effectively stop the spreading of a pile-up after a few breakthroughs. In Figure 4.4 a transmission electron micrograph taken of a thin foil from a 10μ sub-grain specimen after a small plastic strain (0.2%) is shown. Dislocation dipoles are visible in the sub-grain interior.

In summary, it appears that the initial emissions produced in the recovered specimens result from the movement of loosely pinned sub-boundary dislocations. These sources of emission are exhausted, and further emission probably comes from sub-boundary breakthrough events. Only under special circumstances can the breakthrough events give rise to emissions, thus the small number of counts produced as the tensile stress increases beyond the 1 $^{kg}/_{mm^2}$ range. Deformation must procede mostly by the process of dislocation movements and source activations that do not involve more than one or two sub-grains.

4.5 ACOUSTIC EMISSIONS FROM SINGLE CRYSTAL SPECIMENS

Six single crystal specimens were tested, and the orientation of their tensile axes were determined by a Laue back reflection method. Two distinctly different emission behavior patterns were observed. The nature

Figure 4.4. Sub-grain boundaries in an 80% cold rolled, recovered specimen which was strained an additional 0.2% after recovery. 20,000x.

of the pattern depended on whether the specimen was oriented for single or multiple slip.

The absence of grain boundaries in single crystal specimens means that some other unstable dislocation barrier must be operating. One possible mechanism might be the breakthrough of the oxide film on the surface of the specimen by a dislocation pile-up just under the surface. Tatro and Liptai[6] suggested this mechanism, and it may well be the most important one operating in specimens oriented for single slip. Schofield[12] pointed out that some internal barrier must be effective in multiple slip specimens. The formation of Lomer-Cottrell locks by intersecting slip systems would provide such a barrier.

The strength of a Lomer-Cottrell barrier in aluminum is estimated by Stroh[13] There are two mechanisms by which such a barrier may be broken. If the break occurs by dissociation of the sessile dislocation according to

$$\frac{1}{6}a[110]\rightarrow\frac{1}{6}a[2\bar{1}\bar{1}]+\frac{1}{6}a[\bar{1}21]$$

the barrier may support a pile-up of 200 dislocations under an applied stress of 1 $^{kg}/_{mm^2}$. Failure by recombination according to

$$\frac{1}{6}a[112]+\frac{1}{6}a[110]+\frac{1}{6}a[11\bar{2}]\rightarrow\frac{1}{2}a[110]$$

permits the formation of a pile-up of 25 dislocations under an applied shear stress of 1 $^{kg}/_{mm^2}$. The mechanism of failure is dictated by the geometry of the barrier with respect to the pile-up. Seeger's[14] cross slip equation predicts that cross slip may be initiated in aluminum when the local shear stress on a segment of screw dislocation reaches about 190 $^{kg}/_{mm^2}$. Thus,

before failure occurs by dissociation, cross slip should be initiated. Failure by recombination is a possibility.

Assuming that failure by recombination results in the release of an avalanche of about 25 dislocations, a slip area of only $1000\mu^2$ is required to produce a detectable emission. Hence, it is possible that the breaking of sessile dislocation barriers contributed to the emission activity of aluminum single crystals. In cases where cross slip is initiated, a double cross slip dislocation source may be activated. Such a source could also be detectable.

The acoustic emission behavior of the multiple slip single crystal specimens was similar to polycrystal specimens of 1000μ or larger grain size. This was because the dominant slip obstacles operating in both cases were the same. For large grain sizes, the grain boundaries are less significant and internal obstacles such as sessile barriers dominate.

5.0 CONCLUSIONS

Based on acoustic emission observations, stress-strain data, and micrographic evidence, the following conclusions may be drawn concerning the deformation of 99.99% Al.

1.) There appears to be no correlation between grain size and acoustic emission activity in the microstrain regime. The magnitude of the bursts that do occur is nearly always less than 0.2 volts, after amplification. These observations suggest that the dominant slip obstacles during microstrain are intragranular, probably being forest dislocations. The grain boundaries act neither as important slip obstacles, nor as sources of dislocations.

2.) The microstrain theory of Bilello and Metzer[1] is probably applicable to the case of 99.99% aluminum. This theory can explain both the

observed stress-strain behavior, and the acoustic emission behavior.

3.) High-rate-of-emission begins at a stress which does not seem to vary with grain size. This observation, in conjunction with dislocation pile-up observations, suggests that the onset of macro-yielding occurs with the help of dislocation pile-ups held up by grain boundaries. The length of these pile-ups is independent of grain size for grains that are larger than about 200μ in diameter.

4.) From critical analyses of acoustic emission data collected during macrostrain, it is inferred that the emissions result from the activation of dislocation sources near the grain boundaries.

5.) The recovered specimens behave in a distinctly different manner than the recrystallized specimens, from the standpoint of both acoustic emission behavior, and stress-strain behavior. The comparatively large number of emissions detected by applied tensile stress levels below about 1 $^{kg}/_{mm^2}$ are attributed to the early movement of loosely pinned dislocation segments, possibly from the sub-grain walls. The decreased rate of emission with the application of higher stresses is most likely due to an exhaustion of these dislocation segments.

The following conclusions may be drawn concerning the deformation and acoustic emission behavior of 99.9% Cu.

1.) The theory developed to account for the effect of grain size on acoustic emission behavior during the macrostrain regime of 99.99% Al may be applied to account for the observations made on 99.9% Cu. However, the theory should be altered in some of its details to allow for the effect of the larger impurity concentration of 99.9% Cu.

2.) No acoustic emission activity was observed during microstrain in 99.9% Cu due to the presence of impurities.

REFERENCES

1. Bilello, J. C., and Metzger, M., "Microyielding in Polycrystalline Cu," Transactions AIME, 245, (1969), p. 2279.

2. Li, J. C. M., "Petch Relation and Grain Boundary Sources," Trans. AIME, 227, (1963), p. 239.

3. Bill, R. C., "An Acoustic Emission Study of the Deformation Mechanisms of Polycrystalline Aluminum and Copper," Ph.D. Thesis, University of Michigan, Ann Arbor, Michigan, (1970).

4. Perryman, E. W. C., "Relationship Between Recovery and Recrystallization in Superpurity Al," Trans AIME, 203, (1955), p. 1053.

5. Westmacott, K. H., "Hardening in Quenched Al," Philosophical Magazine, Series 8, 14, (1966), p. 239.

6. Liptai, R. G., and Tatro, C. A., Acoustic Emission - A Surface Phenomenon, Symposium on Nondestructive Testing of Aircraft and Missile Components, (1963).

7. Agarwal, A. B. L., "An Investigation of the Behavior of Acoustic Emissions from Metals and a Proposed Mechanism for its Generation," Doctoral Thesis, The University of Michigan, (March, 1968).

8. Friedel, J., Dislocations, Addison Wesley Publishing Company Inc., Oxford, (1964), p. 223.

9. Cottrell, A. H., Dislocations and Plastic Flow in Crystals, Oxford at the Clarendon Press, London, (1953), p. 116.

10. Hirth, J. P., and Lothe, J., Theory of Dislocations, McGraw-Hill Book Co., New York, (1968), p. 683.

11. Friedel, J., Dislocations, Addison Wesley Publishing Company Inc., Oxford, (1964), p. 263.

12. Schofield, B. H., Acoustic Emission Under Applied Stress, Technical Documentary Report No. ASD-TDR-G3-509, Parts I and II, (May, 1964), Contract No. AF33 (657)-8562.

13. Stroh, A. N., "Strength of Lomer-Cottrell Sessile Dislocations," Philosophical Magazine Series 8, 1,)1956), p. 489.

14. Seeger, A., Dislocations and Mechanical Properties of Crystals, Wiley, New York, (1957).

15. Agarwal, A. B. L., Frederick, J. R., and Felbeck, D. K., "Detection of Plastic Microstrain in Aluminum by Acoustic Emissions," Metallurgical Transactions, ASM, 1, No. 4, (April, 1970), p. 1069.

16. Thomas, D. A. and Averbach, B. L., "The Early Stages of Plastic Deformation in Cu," ACTA Metallurgica, 7, (1959), p. 69.

REPORT DISTRIBUTION LIST

1. Mr. John F. Moore
North American Rockwell Corp.
Los Angeles Division
International Airport
Los Angeles, Calif. 90009

2. Dr. J.R. Frederick
University of Michigan
Dept. of Mechanical Engineering
2046 East Engine ring
Ann Arbor, Michigan 48105

3. Mr. Carl Hartbower
Aerojet Solid Propulsion Co.
P.O. Box 13400
Sacramento, Calif. 95813

4. Professor R.H. Chambers
Dept. of Physics
Engineering Experiment Station
Univ. of Arizona
Tucson, Arizona 85721

5. Professor Stuart A. Hoenig
Dept. of Electrical Engineering
Engineering Experiment Station
Univ. of Arizona
Tucson, Arizona 85721

6. Mr. Eugene Roffman
Frankford Arsenal
Fire Control Laboratories
Philadelphia, Pa. 19137

7. Mr. Solomon Goldspiel
U.S. Naval Applied Science Laboratory
Flushing and Washington Avenues
Brooklyn, N.Y. 11251

8. Mr. Otto Gericke
Test and Evaluation Methods
Army Material Command
Army Materials & Mechanics Research Center
Watertown, Massachusetts 02172

9. Mr. D.D. Skinner
Fellow Engineer
Westinghouse Electric Corp.
Research Laboratories
Pittsburgh, Pa. 15235

10. Lt. Col. Louis Klinker, U.S. Army
Office Chief of Research & Development
Materials Science & Technology Branch
Highland Building
3045 Columbia Pike
Arlington, Virginia 22204

11. Mr. Edward Criscuolo
Naval Ordinance Laboratory
Radiation Physics Division (code 223)
White Oak
Silver Spring, Maryland 20910

12. Mr. Stephen D. Hart
Naval Research Laboratory
Mechanics Division
Washington, D.C. 20390

13. Dr. A.S. Tetelman, Head
Materials Division
College of Engineering
Univ. of California
Los Angeles, Calif. 90024

14. Dr. L.W. Orr
Dept. of Electrical Engineering
Univ. of Michigan
Ann Arbor, Michigan 48105

15. Professor Emmett N. Leith
Dept of Electrical Engineering
Univ. of Michigan
Ann Arbor, Michigan 48105

16. Mr. F.S. Williams
Aero Materials Dept.
Naval Air Development Center
Warminster, Pa. 18974

17. Mr. J.L. Kreuzer
Optical Group
Perkin-Elmer
Norwalk, Connecticut 06850

18. Professor R.C. McMasters
Nondestructive Testing Research Lab
Dept. of Welding Engineering
The Ohio State University
Columbus, Ohio 43210

19. Dr. Volker Weiss
Assoc. Chairman
Dept. of Chemical Engineering
& Metallurgy
Syracuse University
Syracuse, New York 13210

20. Professor Lawrence Mann, Jr.
Dept. of Mechanical, Aerospace, &
Industrial Engineering
Louisiana State Univ.
Baton Rouge, Louisiana 70803

21. Mr. Howard A. Johnson
The Boeing Company
Space Division, Aerospace Group
Kent Facility
P.O. Box 3868
Seattle, Washington 98124

22. Mr. C. Gerald Gardner
Southwest Research Institute
8500 Culebra Road
San Antonio, Texas 78206

23. Mr. Carlton H. Hastings
Chief, NDT Evaluation
AVCO Corp., Space Systems Div.
Lowell Industrial Park
Lowell, Mass 01851

24. Mr. David Driscoll
U.S. Army Materials & Mechanics
Research Center
Watertown, Mass 02172

25. Dr. R.L. Gause
Materials Division
Marshall Space Flight Center
Huntsville, Alabama 35800

26. 3 copys to:
Air Force Materials Laboratory, LLN
Attn: Lt. James W. Bohlen
WPAFB, Ohio 45433

27. 20 copys to:
Defense Documentation Center DDC
Cameron Station
Alexandria, Virginia 22314

28. 3 copys to:
Director of Advanced Research
Projects Agency
Washington, D.C. 20301

29. The Institute for Defense Analysis
400 Army-Navy Drive
Arlington, Virginia 22202

30. The Nondestructive Testing
Information Service
Watertown Arsenal
Watertown, Mass 02172

31. Dr. Pravin G. Bhuta, Manager
Applied Mechanics Laboratory
Systems Group of TRW Inc.
One Space Park
Redondo Beach, Calif. 90278

32. Mr. T. Theodore Anderson
Argonne National Laboratory
Reactor Engineering Division
D308
9700 S. Cass Avenue
Argonne, Ill 60439

33. Mr. Phil Hutton & D.C. Worlton
Battelle-Northwest
P.O. Box 999
Richland, Washington 99352

34. Mr. Robert Moss
Boeing Scientific Research Lab.
1-8000
MS 01-14
Box 3981
Seattle, Washington 98124

35. Mr. Charles Musser
The Boeing Company
Saturn Booster Branch
Org. 5-1752
MS LE-62
Box 29100
New Orleans, La. 70129

36. Mr. Harvey L. Balderston
The Boeing Company
Space Division, Kent Facility
P.O. Box 3868
Seattle, Washington 98124
Attn: Orgn. 2-5022
Mail Stop 84-38

37. Mr. Thomas F. Drouillard
Dow Chemical Co.
Rocky Flats Division
P.O. Box 888
Golden, Colorado 80401

38. Mr. R.E. Ringsmuth
Jet Propulsion Laboratory
California Institute of Technology
4800 Oak Grove Drive
Pasadena, Calif 91103

39. Mr. Dwight Parry
Phillips Petroleum
P.O. Box 2067
Idaho Falls, Idaho 83401

40. Mr. Brad Schofield
Teledyne Materials Research
303 Bear Hill Road
Waltham, Mass 02154

41. Mr. Hal Dunegan
Dunegan Research Corp.
2044 Research Drive
Livermore, Calif. 94550

42. Mr. C.D. Bailey
Lockheed-Georgia Co.
Materials Development Laboratory
Dept. 72-14
Marietta, Georgia 30060

43. Mr. R.F. Saxe
North Carolina State Univ.
Nuclear Engineering Dept.
P.O. Box 5636
Raleigh, N.C. 27607

44. Mr. John G. Sessler
Materials Science
Syracuse University Research Corp.
Merrill Lane
Syracuse, N.Y. 13210

45. Mr. L.J. Chockie
General Electric Company
175 Curtner Avenue
San Jose, Calif 95125

46. Lawrence Radiation Laboratory
Attn: Technical Information Dept L-3
P.O. Box 808
Livermore, Calif 94550

47. Mr. James Bryant
Office Chief of Res. & Development
Attn: CROPES
3045 Columbia Pike
Arlington, Va. 22204

48. Mr. H.E. Pearce
McDonnell Douglas Corporation
1100 17th Street, N.W.
Washington, D.C. 20036

49. Mr. Jay M. Stevens
Naval Air Systems Command
Code AIR-52055
Washington, D.C. 20360

50. Mr. Steve Ezangelites
Dept. 263, Mail Station 8
McDonnell Douglas, Western Division
3000 Ocean Park
Santa Monica, Calif 90406

51. Dr. Harold Berger
Group Leader, Nondestructive Testing
Metallurgy Division
Argonne National Laboratory
9700 South Cass Avenue
Argonne, Ill. 60439

52. Dr. Karl Graff
The Ohio State University
Engineering Mechanics Department
212 Boyd Laboratory
155 W. Woodruff Avenue
Columbus, Ohio 43212

53. Mr. J.C. Spanner
NDT Consultant, FFTF Project
Battelle Memorial Institute
Pacific Northwest Laboratories
P.O. Box 999
Richland, Washington 99352

54. Dr. George Martin
Branch Chief
Advanced Fabrication Development Dept
A253, Mail Station 5
McDonnell Douglas Astronautics
Santa Monica, California 90506

55. Mr. Frank J. Sattler, T/M 3355
Materials Development Department
TRW, Inc
23555 Euclid Avenue
Cleveland, Ohio 44117

56. Mr. Alvin Jacobs
Rocketdyne, Inc.
6633 Canoga Ave.
Canoga Park, Calif. 91304